BRIGHAM YOUNG UNIVERSITY

GEOLOGY STUDIES

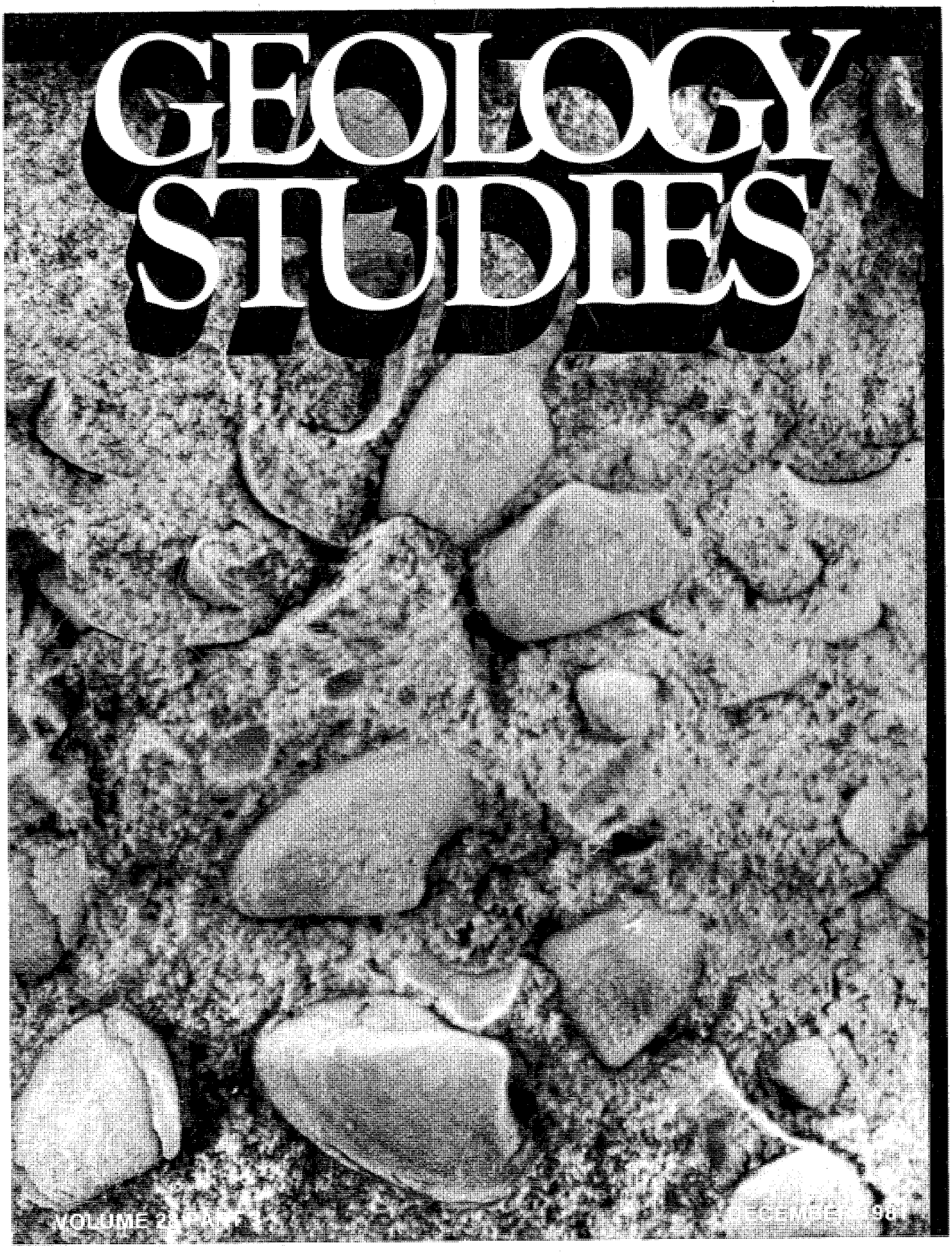

VOLUME 2[illegible] DECEMBER 19[illegible]

Brigham Young University Geology Studies

Volume 28, Part 3

CONTENTS

Three Creeks Caldera, Southern Pavant Range, Utah ..... Thomas A. Steven

Biostratigraphy of the Great Blue Formation ..... Alan K. Chamberlain

Carbonate Petrology and Depositional Environments of the Sinbad Limestone Member of the Moeknopi Formation in the Teasdale Dome Area, Wayne and Garfield Counties, Utah ..... James Scott Dean

Geology of the Antelope Peak Area of the Southern San Francisco Mountains, Beaver County, Utah ..... Vince L. Felt

The Tintic Quartzite in Rock Canyon, Utah County, Utah: A Model for Shallow-shelf Sedimentation ..... Craig D. Hall

Geology of the Longlick and White Mountain Area, Southern San Francisco Mountains ..... Dan E. Haymond

Geology of the Auburn 7½′ Quadrangle, Caribou County, Idaho, and Lincoln County, Wyoming ..... David E. Jenkins

Carbonate Petrology and Depositional Environments of the Limestone Member of the Carmel Formation, near Carmel Junction, Kane County, Utah ..... Douglas W. Taylor

Cover: Slab of bivalves showing Myalina-Pleuroma *suite, from Torrey section, Sinbad Limestone Member, Moenkopi Formation in the Teasdale Dome Area, Wayne County, Utah. Photo courtesy James Scott Dean.*

A publication of the
Department of Geology
Brigham Young University
Provo, Utah 84602

Editors

W. Kenneth Hamblin
Cynthia M. Gardner

Brigham Young University Geology Studies is published by the Department of Geology. This publication consists of graduate student and faculty research within the department as well as papers submitted by outside contributors. Each article submitted by BYU faculty and outside contributors is externally reviewed by at least two qualified persons.

ISSN 0068-1016

Distributed December 1981

12-81 600 52593

CONTENTS

Three Creeks Caldera, Southern Pavant Range, Utah, by Thomas A. Steven 1
Abstract 1
Introduction 1
Regional setting 2
Three Creeks Tuff Member 2
Evolution of the Three Creeks Caldera 4
Comparisons 5
References 7
Figures
1. Geologic map 1
2. Distribution of Three Creeks Tuff Member 2
3. View into subsided block of caldera 3
4. View of topographic wall 4
5. Interpreted relations 4
6. Talus-landslide breccia 5
7. Talus breccia along topographic wall of caldera 6
8. Grooves on topographic wall of caldera 6
9. Ternary diagram 7

Biostratigraphy of the Great Blue Formation, by Alan K. Chamberlain 9
Introduction 9
Location and purpose 9
Previous work 9
Fieldwork 9
Laboratory work 9
Depositional environment of the Great Blue Formation 9
Acknowledgments 10
Stratigraphic sections 10
Oquirrh Mountain section (1) 10
Onaqui Mountain section (2) 11
Ochre Mountain section (3) 11
Boulter Peak (4) 12
Wasatch Mountain section (5) 12
Wellsville Mountain section (6) 14
Fossils 14
Conodonts 14
Corals 14
Brachiopods 14
Bryozoans 14
Sponge 14
Cephalopods 16
Plants 16
Other fossils 16
Conclusion 16
References cited 17
Figures
1. Index map 9
2. Oquirrh Mountain (section 1) 10
3. Onaqui Mountain (section 2) 11
4. Ochre Mountain (section 3) 12
5. Boulter Peak (section 4) 13
6. Wasatch Mountains (section 5) 13
7. Wellsville Mountain (section 6) 14
8. East-west correlation 16
Table
1. First and last occurrences of organisms in the Great Blue Formation 15

Carbonate Petrology and Depositional Environments of the Sinbad Limestone Member of the Moenkopi Formation in the Teasdale Dome Area, Wayne and Garfield Counties, Utah, by James Scott Dean 19
Abstract 19
Introduction 19
Location 19
Methods and terminology 20
Field methods 20
Laboratory methods 20
Terminology 20
Previous work 22
Geologic setting 22
Acknowledgments 23
Geometry and petrology of carbonate lithofacies 23
Lithofacies A 23
Stromatolitic boundstone subfacies 24
Oolite-peloid packstone subfacies 25
Dolomicrite subfacies 26
Channel conglomerate subfacies 26
Evaporite subfacies 26
Lithofacies B 28
Skeletal packstone subfacies 28
Pelletal wackestone subfacies 30
Lithofacies C 30
Lithofacies D 33
Oolite-mollusk packstone subfacies 33
Peloidal mudstone-wackestone subfacies 34
Lithofacies E 34
Lithofacies F 36
Correlation of lithofacies 36
Paleontology 37
Ichnology 37
Diagenesis 37
Recrystallization 38
Dolomitization 38
Homogeneous dolomites 38
Heterogeneous dolomites 38
Depositional environments of carbonate lithofacies 39
Lithofacies A 39
Stromatolitic boundstone subfacies 39
Oolite-peloid packstone subfacies 40
Dolomicrite subfacies 41
Channel conglomerate subfacies 41
Evaporite subfacies 41
Lithofacies B 41
Lithofacies C 42
Lithofacies D 42
Lithofacies E 42
Lithofacies F 43
Depositional summary 43
Petroleum potential 44
Potential of lithofacies 45
Appendix 45
References cited 45
Figures
1. Index map 19
2. Outcrop of Sinbad Limestone Member 20
3. Fence diagram: stratigraphic relationships 21

4. Stratigraphic sections ..... in pocket
5. Classification of carbonate rocks 21
6. A.–Paleotectonic features 23
B.–Paleogeography and sedimentary facies 23
7. Photomicrograph: stromatolitic boundstone 24
8. Slab showing cryptalgal dolomicrite 24
9. Photomicrograph: recrystallized packstone fabric 25
10. Photomicrograph: packstone from Torrey section 25
11. Photomicrograph: cryptalgal dolomicrite 26
12. A.–High-angle cross-bedding 27
B.–Carbonate flaser bedding 27
C.–Channel conglomerate 27
D.–Cryptalgal dolomicrite 27
E.–Herringbone cross-bedding 27
F.–Herringbone cross-sets 27
13. Flat-pebble and subrounded intraclasts 28
14. Rippled and gypsiferous dolomicrite 28
15. A.–Cyclic bioturbation 29
B.–Tidal channel 29
C.–Skeletal packstone 29
D.–Tidal channel 29
E.–Planar cross-bedding 29
F.–Massive ptygmatic gypsum 29
16. Photomicrograph: massive gypsum 30
17. Photomicrograph: pelletal wackestone 30
18. Photomicrograph: grainstone layer 30
19. Photomicrograph: umbrella structure 30
20. Photomicrograph: *Skolithos* burrow filled with debris 31
21. Photomicrograph: mollusk wackestone 31
22. A.–View of Grand Wash section 32
B.–Contact between claystone and shales 32
C.–Teepee ridges 32
D.–Ripple marks 32
E.–Limestones held up by channeled dolomites 32
23. Photomicrograph: remnant lamination in dolomite .. 33
24. Photomicrograph: recrystallized skeletal packstone 33
25. Photomicrograph: dissolution surface, packstone and wackestone 34
26. Sinbad Limestone Member 34
27. Photomicrograph: heterogeneous dolomite 35
28. Photomicrograph: dolomitized oolite grainstone 35
29. Photomicrograph: dolomite fabric 35
30. Photomicrograph: dolomicritized peloids 35
31. View of tidal channel 36
32. Diagram: relationships of depositional environments 40
33. A.–Transgressing tidal flat-sabka 43
B.–Subtidal deposition of second phase 43
C.–Final phase of deposition 43

Plates
1. Ammonoids, gastropods, bivalves 49
2. Bioturbation, sponge, spicule net 51

Geology of the Antelope Peak Area of the Southern San Francisco Mountains, Beaver County, Utah, by Vince L. Felt 53

Introduction 53
Objectives 53
Location 53
Previous work 54
Geologic setting 54
Acknowledgments 54
Stratigraphy 54
General statement 54
Dacite of Shauntie Hills 54
Needles Range Formation 54
Wah Wah Springs Tuff Member 55
Lund Tuff Member 55
Wallaces Peak Tuff Member 55
Isom Formation 55
Formation of Blawn Wash 55
Tuff Member of Sevey's Well 55
Quartz Latite Member of Squaw Peak 56
Lower tuff member 56
Sandstone member 57
Upper tuff member 57
Rhyolite flow member 57
Lava flow member 57
Basaltic conglomerate 57
Basalt flow 57
Lower conglomerate 58
Upper conglomerate 58
Alluvium 58
Structure 58
General statement 58
Northeast-trending faults 58
Northwest-trending faults 58
East-trending faults 59
Eruptive centers 59
Age of faulting 59
Oligocene to early Miocene faulting 59
Mid-Miocene faulting 59
Post mid-Miocene basin-and-range faulting 60
Summary 60
Geologic history 60
Early Tertiary to middle Oligocene 60
Middle Oligocene to late Oligocene 60
Early Miocene to Recent 60
Miocene depression 62
Alteration 63
Conclusions 64
References 65

Figures
1. Index map of the Antelope Peak area 53
2. Correlation of map units 55
3. Tuff Member of Sevey's Well 56
4. Quartz Latite Member of Squaw Peak showing rypical spheroidal weathering and popcorn texture 56
5. Photomicrograph (crossed nicols): Quartz Latite Member of Squaw Peak 56
6. Photomicrograph (crossed nicols): xenocrysts of subhedral plagioclase enclosed in a reaction rim 57
7. Photomicrograph (crossed nicols): felted matrix of plagioclase microlites in the basalt flow unit 58
8. Map of fault patterns and intensely altered rocks 59
9. Diagrammatic cross section, illustrating the concept of northeast-striking subordinate listric faults 59
10. Regional geologic map 61
11. Gravity map, southern San Francisco Mountains 62
12. Autoclastic breccia unit, Quartz Latite Member of Squaw Peak 63
13. Approximate location of Miocene depression 63
14. Magnetic map 64

Plate
1. Geologic map of the Antelope Peak area ..... in pocket

The Tintic Quartzite in Rock Canyon, Utah County, Utah: A Model for Shallow-shelf Sedimentation, by Craig D. Hall 67

Introduction 67
Location of study area 67
Methods of study 67
Previous work 68
Acknowledgments 68
Lithology 68
Sedimentary structures 69
Biogenic sedimentary structures 69
Interpretation 69
Cross-bedding analysis 71
Vertical successions 72
Deposition of the Tintic Quartzite 75
Other examples of clastic sedimentation 75
Shallow-shelf sedimentation 76
Summary 77
References cited 79
Figures
1. Index map of study sections 67
2. Block diagram of planar cross-bedding 69
3. Block diagram of trough cross-bedding 70
4. Block diagram of channel features 71
5. Steampower graph 71
6. Velocity vs. grain size graph 72
7. Average current directions in the formation 73
8. Columnar sections of the Tintic Quartzite 74
9. Columnar sections of the Flathead Sandstone 76
10. Columnar section of the Duolbasgaissa Formation, Norway 77
11. Idealized vertical sequence of shallow-shelf, transgressive deposits 79
Table
1. Special fluid depth-velocity quantities and their respective Froude Numbers 70

Geology of the Longlick and White Mountain Area, Southern San Francisco Mountains, by Dan E. Haymond 81
Abstract 81
Introduction 81
Location 81
Previous work 81
Acknowledgments 81
Stratigraphy 82
General statement 82
Devonian System 83
Sevy Dolomite 83
Guilmette-Simonson Dolomite 83
Cove Fort Quartzite 83
Crystal Pass Limestone 83
Pinyon Peak Limestone 83
Mississippian System 83
Monte Cristo Limestone 83
Dawn-Whitmore Wash Limestone Member . 83
Anchor-Thunder Springs Limestone Member 83
Deseret Limestone 85
Humbug Formation 85
Great Blue Limestone 85
Chainman Shale 86
Pennsylvanian System 86
Callville Limestone 86
Permian System 86
Pakoon Limestone 86
Queantoweap Sandstone 86
Toroweap Formation 86
Kaibab Limestone 87
Jurassic System 87
Navajo Sandstone 87
Tertiary System 87
Dacite of Shauntie Hills 87
Needles Range Formation 87
Wah Wah Springs Tuff Member 88
Lund Tuff Member 88
Wallaces Peak Tuff Member 88
Isom Formation 88
Hole-in-the-Wall Tuff Member 88
Formation of Blawn Wash 88
Tuff of Sevey's Well Member 88
Quartz Latite of Squaw Peak Member 88
Lower tuff member 88
Mafic flow member 89
Upper tuff member 89
Rhyolite flow member 89
Formation of Brimstone Reservoir 89
Alluvial cover 89
Structure 89
General statement 89
Thrust faults 89
East-west-trending faults 89
North-south-trending faults 90
Northeast-southwest-trending faults 90
Northwest-southeast-trending faults 90
Folds 90
Alteration 90
Mineralization 91
Geologic history 91
Economic potential 94
Appendix 94
References cited 99
Figures
1. Index map 81
2. Composite Paleozoic section 82
3. Paleozoic correlation diagram 84
4. Great Blue Limestone at White Mountain 85
5. Overturned section of Pakoon Formation and Callville Limestone 86
6. Toroweap and Kaibab Limestone at Miners Hill 87
7. Aerial view of the Brimstone Lineament 90
8. Monocline in the Humbug Formation 91
9. Hydrothermal bleaching along a joint 92
10. Silicified upper tuff member 92
11. Brimstone sinter mound 93
12. Fumarole lined with native sulfur 93
Plate
1. Geology of the Longlick and White Mountain area .. in pocket

Geology of the Auburn 7½′ Quadrangle, Caribou County, Idaho, and Lincoln County, Wyoming, by David E. Jenkins 101
Introduction 101
Previous work 101
Method of study 101
Acknowledgments 101
Stratigraphy 102
General statement 102
Permian System 102
Phosphoria Formation 102
Rex Chert Member 102

Triassic System 102
Dinwoody Formation 102
Woodside Formation 103
Thaynes Formation 103
A member 103
B member 104
Portneuf Limestone Member 104
Lower member of the Thaynes Formation 104
Upper member of the Thaynes Formation 104
Ankareh Formation 104
Lanes Tongue of the Ankareh Formation 104
Wood Shale Tongue of the Ankareh Formation 104
Ankareh Formation of the Absaroka Plate 104
Higham Grit 104
Jurassic System 105
Nugget Sandstone 105
Twin Creek Limestone 105
Preuss Sandstone 105
Stump Sandstone 106
Cretaceous System 106
Ephraim Conglomerate 107
Peterson Limestone 107
Bechler Conglomerate 107
Draney Limestone 107
Tygee Member of the Bear River Formation 107
Wayan Formation 108
Tertiary System 108
Salt Lake Formation 108
Quaternary System 108
Structure 108
General statement 108
Meade Thrust Fault 109
Faults 109
Tear faults 109
Transverse faults 109
North-south high-angle faults 109
Folds 109
Economic geology 111
Petroleum 111
Phosphate 112
Hot springs 112
Other deposits 112
Summary 112
Appendix 112
References 116
Figures
1. Index map 101
2. Generalized stratigraphic column 102
3. Rex Chert Member of the Phosphoria Formation 103
4. Member divisions Thaynes-Ankareh Formations 103
5. Ammonites of the Thaynes Formation 104
6. Twin Creek Limestone 105
7. Twin Creek Limestone 106
8. Ripple marks, Stump Sandstone 106
9. Ripple marks, Stump Sandstone 107
10. Slickensides, Ephraim Conglomerate 107
11. Tygee Member of the Bear River Formation 108
12. Salt Lake Formation 108
13. Salt Springs Stump Valley 108
14. Thrust fault zones, Idaho-Wyoming 110
15. Imbrication of footwall 111
16. Spring Creek Syncline 112
17. Active hot springs 112
Plate
1. Geologic map of the Auburn Quadrangle ..... in pocket

Carbonate Petrology and Depositional Environments of the Limestone Member of the Carmel Formation, near Carmel Junction, Kane County, Utah, by Douglas W. Taylor 117
Abstract 117
Introduction and geologic setting 117
Location 118
Methods of study and nomenclature 118
Previous work 118
Acknowledgments 119
Geometry and petrology of lithofacies 119
Lithofacies A 119
Lithofacies B 119
Siltstone subfacies 119
Dolomicrite subfacies 119
Stromatolitic boundstone subfacies 119
Evaporite dolomicrite subfacies 120
Lithofacies C 121
Oolite skeletal packstone and grainstone subfacies 121
Bivalve wackestone subfacies 121
Lithofacies D 122
Lithofacies E 122
Lithofacies F 123
Peloidal grainstone subfacies 124
Stromatolitic boundstone subfacies 124
Correlation 125
Paleontology 125
Ichnology 126
Diagenesis 126
Recrystallization 126
Dolomitization 127
Depositional environments of lithofacies 127
Lithofacies A 127
Lithofacies B 128
Dolomicrite subfacies 128
Stromatolitic boundstone subfacies 128
Evaporite subfacies 129
Lithofacies C 129
Lithofacies D 129
Lithofacies E 129
Lithofacies F 129
Depositional summary 129
Petroleum potential 131
Appendix 131
References cited 133
Figures
1. Index map 117
2. Paleogeographic map 118
3. Carmel Limestone Member 118
4. Nine measured sections ..... in pocket
5. Photomicrograph: dolomitic siltstone subfacies 120
6. Photomicrograph: thinly bedded dolomicrite 120
7. Cryptalgal bedding 120
8. Photomicrograph: stromatolitic boundstone 120
9. Photomicrograph: nodular anhydrite and dolomicrite 121
10. Cross-bedded oolite-skeletal packstone 121
11. Drawing: possible bryozoan colony 121
12. Photomicrograph: oolite-skeletal packstone 122
13. Encrinal grainstone 122

14. Weathered surface of packstone 122
15. Echinoid spines 122
16. (A) *Diademopis,* (B) *Ostrea (Liostrea) strigulecula,* (C) *Gryphaea* valve, (D) *Cossmannea imlayi,* (E) *Lima (Plagiostoma) zonia* valve, (F) possible cyclostome bryozoan colony, (G) coelenterate ? colony, (H) *Lima (Plagiostoma) occidentalis* valve, (I) *Mesenteripora* encrusting *Ostrea* shell 123
17. Photomicrograph: wackestone subfacies 124
18. Wackestone subfacies 124
19. Units exposed in roadcut 124
20. Photomicrographs: (A) argillaceous mudstone and (B) micro-cross-bedding 125
21. Photomicrograph: peloidal grainstone 126
22. Photomicrograph: peloidal grainstone 126
23. Ripple marks in dolomicrite 126
24. Photomicrograph: packstone 126
25. Photomicrograph: partially recrystallized oolites 127
26. Depositional model for the Carmel Limestone Member 128
27. Ripple marks 130
28. Bivalve coquina 130
29. Transgressive oolite shoals, phase I; regression of sea and prograding shale, phase II; minor transgression of peloidal grainstones, phase III 130
30. Generalized stratigraphic column 131

Publications and maps of the Geology Department 135

Carbonate Petrology and Depositional Environments of the Sinbad Limestone Member of the Moenkopi Formation in the Teasdale Dome Area, Wayne and Garfield Counties, Utah*

JAMES SCOTT DEAN
Shell Oil Company
P.O. Box 831
Houston, Texas 77001

ABSTRACT.–The Sinbad Limestone Member of the Moenkopi Formation in the Teasdale Dome records a major southeastern advance of carbonate sedimentation during Early Triassic (Scythian) time. Three principal depositional phases are recognized.

The transgressive tidal flat-sabka of the earliest phase is characterized by deposition of stromatolitic boundstone and nodular to bedded gypsum in the high intertidal-supratidal zone; oolite-peloid packstone and intrafacies conglomerate in channels of the intertidal zone; and laminate to cryptalgal dolomicrites from tidal flats and intrachannel pods. Pervasive syngenetic dolomitization and an impoverished molluscan fauna document hypersaline conditions.

Subtidal deposition of the second phase occurred during the period of maximum transgression of the Sinbad seaway. Pelletal wackestones and cyclically bioturbated skeletal packstones with interbeds of storm-surge grainstones were deposited in shoal-protected lagoons which graded shoreward into cross-bedded bars of coated grains from tidal channels. Peloidal mudstones and wackestones with a fairly diverse ammonoid fauna and lyssakid sponges record sub-wave-base deposition under near-normal marine salinities, farther out on the shelf.

Well-sorted, oolite-peloid grainstones of the final regressive phase accumulated on moderate-energy shoals which paralleled the retreat of the Sinbad shoreline to the north and west. Grainstones are rippled and herringbone cross-bedded and exhibit intense but variable dolomitization.

Porosity in the Sinbad Member is variable from lithofacies to lithofacies but is generally fabric selective and dependent upon diagenetic enhancement: mainly dolomitization, leaching, and fracturing.

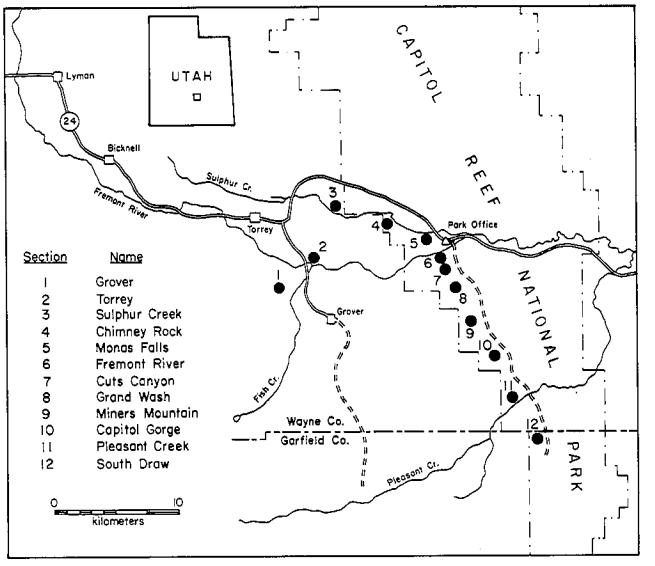

FIGURE 1.–Index map of study area showing location of measured sections.

INTRODUCTION

The Lower Triassic Sinbad Limestone Member of the Moenkopi Formation is one of a few conspicuous carbonate units in a dominantly clastic redbed sequence in the Colorado Plateau. Excellent exposures of the member occur around the flanks of the Teasdale Dome, within and adjacent to Capitol Reef National Park in Wayne and Garfield Counties in south central Utah. Deposited in a variety of supratidal to subtidal environments, the dolomite, limestone, and dolomitic claystone of the Sinbad Member represent a unique and fortuitous opportunity for detailed three-dimensional analysis of a rapid facies change from normal marine to hypersaline conditions.

The primary objective of this study is to describe and interpret the carbonate facies that document this transition and employ the data in the construction of a depositional model. Recent emphasis on the hydrocarbon potential of the Utah hingeline area has stimulated interest in the Sinbad Limestone Member as a prospective petroleum reservoir. Thus, a secondary objective is to petrographically determine the extent and controlling factors for diagenetic changes affecting porosity and permeability within each facies.

Location

The study area is located along the border between the High Plateaus and Canyonlands sections of the Colorado Plateau Province in southern Wayne and northern Garfield Counties, Utah (fig. 1). All twelve measured sections are in canyons along the nose and eastern flank of the Teasdale Dome. The dome is an asymmetrical, doubly plunging anticline of Laramide age, genetically related to and situated between the San Rafael Swell and Circle Cliffs upwarps of south central Utah.

The study area is readily accessible via Utah 24, which connects the headquarters of Capitol Reef National Park with the towns of Loa and Hanksville. The North Grover and Torrey (fig. 2) sections are reached by a well-maintained county road which joins Utah 24 at the Torrey cemetery. The West Sulphur Creek section is best accessible via the old Utah 24, now an unmaintained dirt road, which intersects the present Utah 24 2.4 km east of Torrey, Utah. The Chimney Rock section requires a 1.2-km walk southwest from the Chimney Rock view stop down the gorge to the junction of Sulphur Creek Canyon. The Monas Falls section is located 0.8 km up Sulphur Creek Canyon on a hiking trail which begins just west of the park headquarters near the town of Fruita. The Fremont River, Cuts Canyon, Grand Wash, Miners Mountain, Capitol Wash, and Pleasant Creek sections are accessible via a well-maintained scenic drive road which proceeds south from the park headquarters. These sections require a 0.4- to 1.2-km hike up their respective canyons. The South Draw section is reached via a jeep trail south from Pleasant Creek. Figure 1 shows the location of each measured section, all of which are found within the Townships 29–31 south, and Ranges 5–6 east.

*A thesis presented to the Department of Geology, Brigham Young University, in partial fulfillment of the requirements for the degree Master of Science, December 1980. Thesis chairman: J. Keith Rigby.

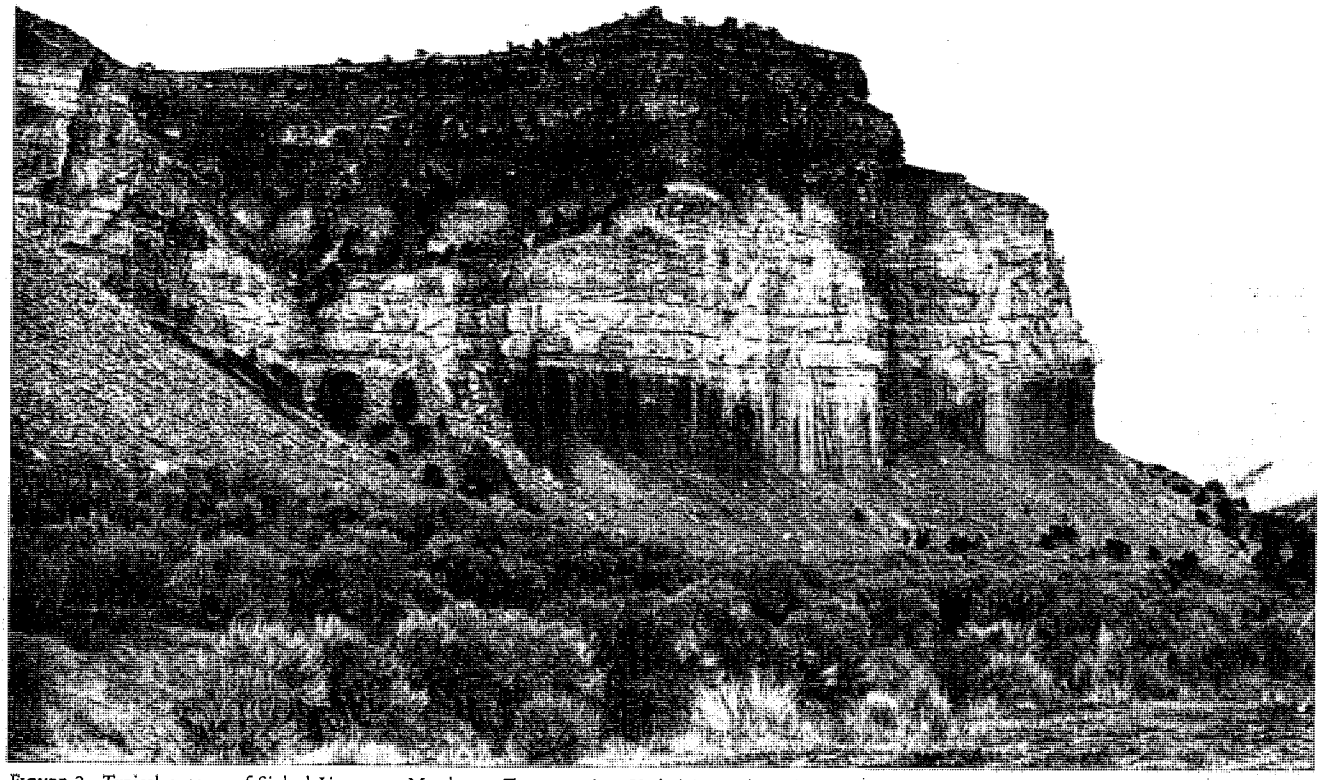

FIGURE 2.–Typical outcrop of Sinbad Limestone Member at Torrey section. Underlying and overlying redbeds are the Black Dragon and Torrey Members of the Moenkopi Formation.

Methods and Terminology

Field Methods

Twelve sections (fig. 3) of the Sinbad Limestone Member were measured with a meter stick or steel tape. Most sections are exposed as cliffs, but, where slopes of more than 1 m were encountered, a Jacob staff was employed. A Brunton compass was used with both methods to insure that beds were measured normal to dip. Each section was described on a centimeter-by-centimeter basis, with paleocurrent directions plotted by azimuth. Handsamples were collected at every significant lithologic change, and special care was taken to sample unweathered rocks. Sections were selected to provide maximum resolution of lateral facies change, with spacing of 1.7–3.4 km. Reconnaissance was carried out during the summer of 1979. Sections were revisited and measured in detail during the fall of 1979 and winter of 1980, as weather would permit, and finished during April and May 1980.

Laboratory Methods

Several hundred field samples were made into polished slabs at Brigham Young University, then etched in dilute HCl and examined under a binocular microscope for fabric and textural relationships. More than 200 thin sections were subsequently prepared from the best slabs, and examined for microsedimentary structures and fossils. A petrographic microscope was also employed for the analysis of constituent mineral grains. Selected slides from each facies were stained to determine the relative amounts of calcite and dolomite present using both Alizarin Red S (Sabins 1962, p. 1184) and ferrocyanide solution (Friedman 1959, p. 95).

Representative samples (averaging 250 g apiece) from each of the six lithofacies were selected from the Torrey, Grand Wash, and South Draw sections (fig. 4) to be analyzed for insoluble residue content. Each sample was weighed and dissolved in dilute HCl. Microcrystalline dolomites were treated with dilute formic acid. Insoluble residues remaining after washing through a 200-mesh screen were dried, weighed, and examined for clastic grain mineralogy.

Samples from lithofacies most likely to contain phosphatic microfossils were crushed and dissolved in dilute formic or glacial acetic acid. The residue was then washed on a 120-mesh screen, dried, and examined under a binocular microscope.

Terminology

Carbonate nomenclature used in this study follows so far as possible the scheme of Dunham (1962) which classifies rocks on the basis of their depositional texture. Rocks such as dolomites, in which the original textures are often obscured, are ignored in Dunham's classification and are here termed crystalline carbonates. The Sinbad Limestone Member is predominantly dolomite throughout the study area, with original textures in varying stages of preservation. Most rocks within the member are adequately described by Dunham's terminology; however, those that are not are included in a separate classification adapted to crystalline fabrics. Figure 5 shows both schemes. Note that although mudstone has commonly been

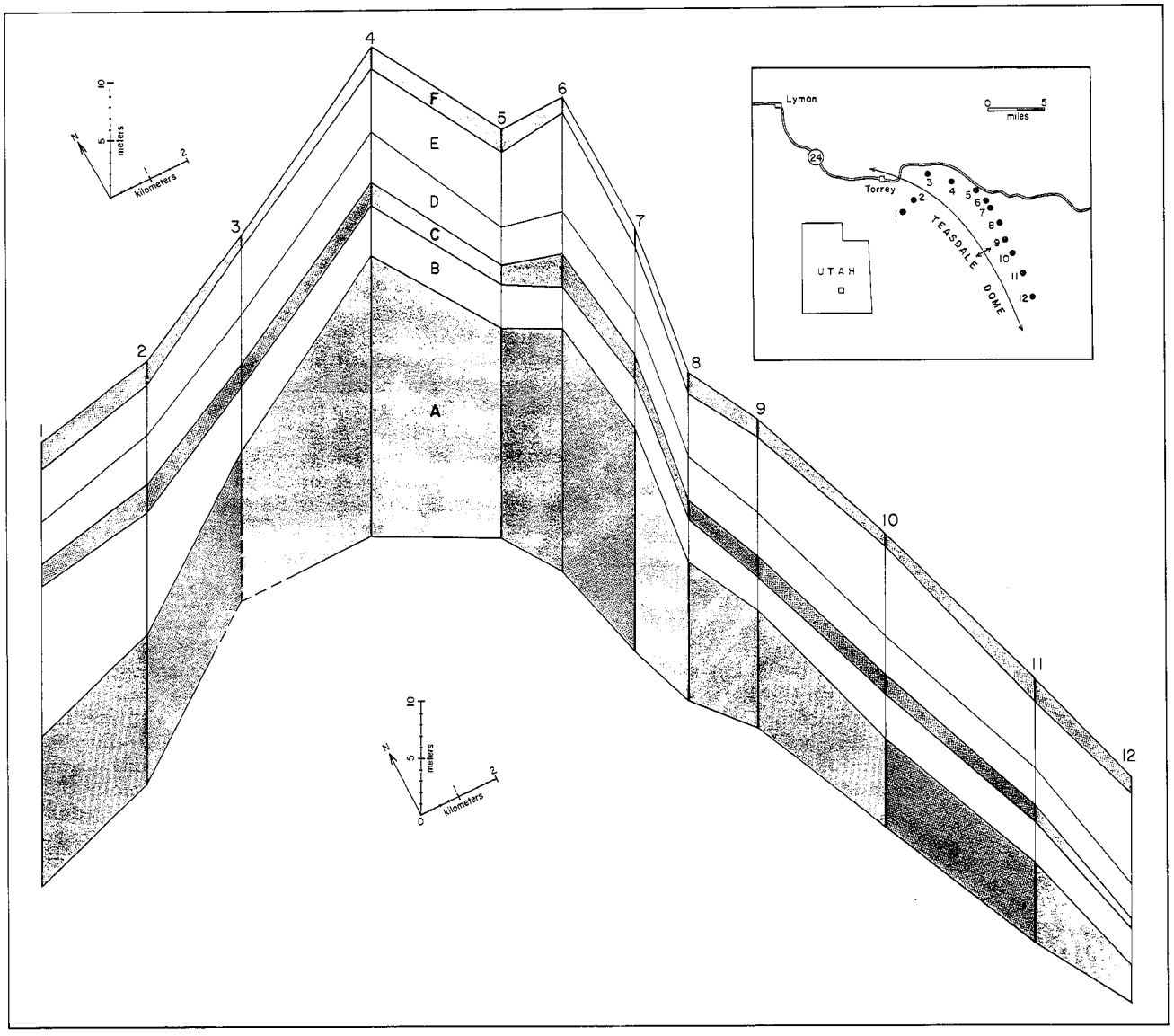

FIGURE 3.–Fence diagram illustrating stratigraphic relationships between lithofacies A–F within the Sinbad Limestone in the study area.

CLASSIFICATION SCHEME FOR CARBONATE ROCKS IN THE SINBAD LIMESTONE MEMBER

Limestones and Dolomites – Depositional Texture recognizable					Dolomites – Depositional Texture not recognizable			
Original components not bound together during deposition				Original components were bound together during deposition	Crystalline Fabric			
Contains mud (particles of clay and fine silt size)			Lacks mud and is grain supported		up to .03 mm	.03 – .06 mm	.06 – .2 mm	more than .2 mm
Mud – supported		Grain supported						
Less Than 10% grains	More Than 10% grains							
MUDSTONE	WACKESTONE	PACKSTONE	GRAINSTONE	BOUNDSTONE	DOLOMICRITE	FINELY CRYSTALLINE DOLOMITE	MEDIUM CRYSTALLINE DOLOMITE	COARSELY CRYSTALLINE DOLOMITE

FIGURE 5.–Classification of carbonate rocks, modified after Dunham (1962), showing size parameters for crystalline dolomites.

used in previous studies to describe fine-grained clastic rocks, consistency dictates that throughout this paper it be used in its carbonate context.

Additional detail is gained by adding modifiers to sufficiently describe each rock. For example, a mollusk-echinoderm wackestone is a mud (micrite)-supported rock with more than 10 percent skeletal grains (allochems) of mollusk and echinoderm affinities.

Asquith (1979, p. 5) warned that problems may arise in distinguishing packstones from grainstones if careful differentiation between spar and neomorphic pseudospar (from micrite) is not consistently made. This distinction is important in petrographic analysis of several grain-supported subfacies within the Sinbad Member where diagenetic recrystallization of a micritic matrix may give the appearance of spar, causing a packstone to be misclassified as a grainstone. Throughout this study, criteria for differentiating spar from pseudospar, as outlined by Asquith (1979) and Folk (1965), were followed.

Petrographic description of allochems generally follows Bathurst (1975), with the following exception. It is useful in the Sinbad rocks, to employ both the term *peloid,* which is irrespective of origin and variable in size, and the term *pellet* as defined by Folk (1962, p. 64) for material probably of fecal origin satisfying the size constraints of 0.03–0.15 mm.

Previous Work

The Sinbad Limestone Member of the Moenkopi Formation was named by Gilluly and Reeside (1928) for distinctive carbonate exposures in the Sinbad area of the San Rafael Swell. Hunt (1953) later suggested certain limestone beds in the lower third of the Moenkopi Formation near the Henry Mountains are equivalent to the Sinbad Member and contain marine fossils which establish their age as Lower Triassic. McKee (1954) completed the first comprehensive regional analysis of the stratigraphy, facies, and depositional environments of the Moenkopi Formation, but emphasized southern Utah and northern Arizona. The Sinbad equivalent in southwestern Uah, the Timpoweap Member, was described as the producing reservoir in the Virgin Oil Field by Bahr (1963). He recognized three facies and briefly discussed the dominant carbonate lithologies.

Smith and others (1963) emphasized the uranium potential of the Capitol Reef area but included the first detailed lithologic description of the Sinbad Limestone Member. They also did minor geochemical work to determine limestone-dolomite ratios and measured and described several sections confirming the westward thickening of the marine sequence. "Sandstones" in the Sinbad Member, as mentioned by Smith and others (1963, p. 12), were searched for in vain by this writer and must refer to clastic-looking, coarsely crystalline dolomites common in the upper ledges. Hawley and others (1968) briefly described the Sinbad Member from the San Rafael Swell, geochemically confirming the local variation in percentage of limestone and dolomite, but made no attempt to determine facies relationships or diagenetic changes.

A second regional study of the Moenkopi Formation was undertaken by Stewart and others (1972) with detailed lithologic and faunal descriptions, including an attempt to correlate the numerous locally recognized units and informal members. The treatment of the Sinbad Limestone Member was limited to a brief overview of depositional parameters and equivalent carbonate beds containing the important *Meekoceras* fauna.

The most comprehensive analysis of the Sinbad Limestone Member, to date, is that of Blakey (1974), who studied the stratigraphy and depositional environments of the Moenkopi Formation in southeastern Utah. He divided the formation into four members, all of which are readily discernible in the study area, and proposed three new members, in addition to the previously proposed Sinbad Member. From oldest to youngest they include (1) Black Dragon, (2) Sinbad, (3) Torrey, and (4) Moody Canyon Members. The Black Dragon and Moody Canyon Members were interpreted to represent clastic-dominated, paralic to transitional marine deposition, and the Torrey Member was thought to be a prograding delta sequence.

The Sinbad Member was described in terms of general carbonate petrology and depositional environment by Blakey (1974) with four regional facies defined, but he (1974, p. 26) did not study it in enough detail in the Teasdale uplift to accurately define facies. During the course of the present study, the facies defined by Blakey, generally in the San Rafael Swell, were found to be less applicable to rock sequences in the Teasdale Dome area. An attempt at correlation of the lithofacies used in the present study and those of Bahr (1963) and Blakey (1974) is included in a separate section of this paper.

Geologic Setting

The depositional history of southeastern Utah during the early Mesozoic was dominated by three principal paleotectonic elements. To the west was the Cordilleran Miogeosyncline, a major subsiding trough up to 640 km wide which extended from present-day northern Canada southward to Baja California. This trough had been the locus of marine sedimentation from Late Precambrian through Early Triassic times, although it was considerably less widespread and dynamic in Triassic time than during the Paleozoic. Bissell (1970) estimated that in the Early Triassic more than 1500 m of combined carbonate and clastic material were deposited in the trough in northern Utah and southern Idaho. South and east of the study area, remnants of the Coloradoan (ancestral Rocky) Mountains continued to supply clastics, as they had since the Middle Pennsylvanian. Stewart and others (1972) considered the principal terrigenous contributors during Moenkopi time to be the Uncompahgre Uplift and Front Range highland of Colorado, the Mogollan highland of central Arizona-New Mexico, and local input from the Defiance (Zuni) and Salt Anticline Uplifts of southeastern Utah. These source areas waned toward the Late Triassic, however, as indicated by the eventual burial of Uncompahgre rocks by the Chinle Formation (Hintze 1973, p. 54). The third element was a broad, gently sloping shelf, situated between the uplands and the miogeosyncline. It was over this shelf that most of the Moenkopi Formation, including the Sinbad Limestone Member, was deposited.

The Moenkopi Formation of Early and Middle Triassic age encompasses a variety of paleoenvironments deposited in several transgressive-regressive phases over much of the present-day Colorado Plateau. Toward the highlands, continental redbeds predominate, and adjacent to the miogeosyncline, marine carbonates make up most of the formation. Several eastward transgressive advances spilled onto the shelf from the miogeosynclinal trough and deposited cycles of carbonate rocks. These are, from oldest to youngest, the Sinbad-Timpoweap Limestone Member, the Virgin Limestone Member, and the gypsiferous Shnabkaib Member. Thicker sequences of redbeds are interfingered with these marine units and represent returns to regressive siliciclastic sedimentation.

The Moenkopi shelf grades northward into the Wyoming platform (Blakey 1974), where lithologically similar rocks of the Chugwater Group were deposited. Both the Moenkopi and Chugwater Formations intertongue westward with the deeper-water shelf carbonates of the Thaynes Limestone (Kummel 1954). Mutual occurrence of the *Meekoceras* fauna and subsurface well data indicate that the Sinbad Limestone Member of the Moenkopi Formation represents a major southeastern tongue of the Thaynes Limestone. Figure 6 illustrates facies relationships and paleogeography of the study area during Early Triassic time.

Acknowledgments

The author extends deep appreciation to Dr. J. Keith Rigby, chairman, for his untiring assistance and encouragement during fieldwork and preparation of the manuscript. I am also grateful to Dr. Lehi Hintze, committee member, for reviewing the manuscript, Drs. W. R. Phillips and H. J. Bissell for assistance on various aspects of petrology, and Dr. M. S. Petersen for assistance in ammonoid identification. The author is grateful to members of the 1980 BYU Geology Summer Camp for invaluable field assistance in measuring and describing sections, and to the McLean and Golden Durfey families for their hospitality and kindness during our stay at their ranch. Special thanks is extended to my wife, Maria, for her constant support and inspiration. A grant from Gulf Oil Company of Casper, Wyoming, helped defray expenses of the study.

GEOMETRY AND PETROLOGY OF CARBONATE LITHOFACIES

The Sinbad Limestone Member of the Moenkopi Formation within the Teasdale Dome study area, is readily divided into six lithofacies (A through F in ascending order) on the basis of combined outcrop and thin-section analysis. Nine subfacies are also recognized to facilitate detailed description and interpretation. The geometry, defining parameters, and general mineralogy are discussed for each lithofacies while petrology and sedimentary structures are introduced by subfacies. A fence diagram (fig. 3) shows the regional thickness trends for each lithofacies.

Lithofacies A

Lithofacies A comprises a suite of heterogeneous dolomites and extends upward from the contact of the Sinbad Limestone Member with the underlying Black Dragon Member (fig. 4) to the lowest occurrence of predominantly skeletal limestones and dolomitic limestones of lithofacies B. The regional southeastward thinning of the Sinbad Member is best reflected in the rapid thickness change of lithofacies A (fig. 3). The lithofacies thins from 24.75 m, well over half the total section at Chimney Rock, to a thickness of only 3.25 m in the South Draw section, a decrease of 21.5 m in less than 22 km.

The lower contact of the facies and member is conspicuous throughout the study area and is marked in most sections by a lithologic break from pale reddish brown silty shale of the un-

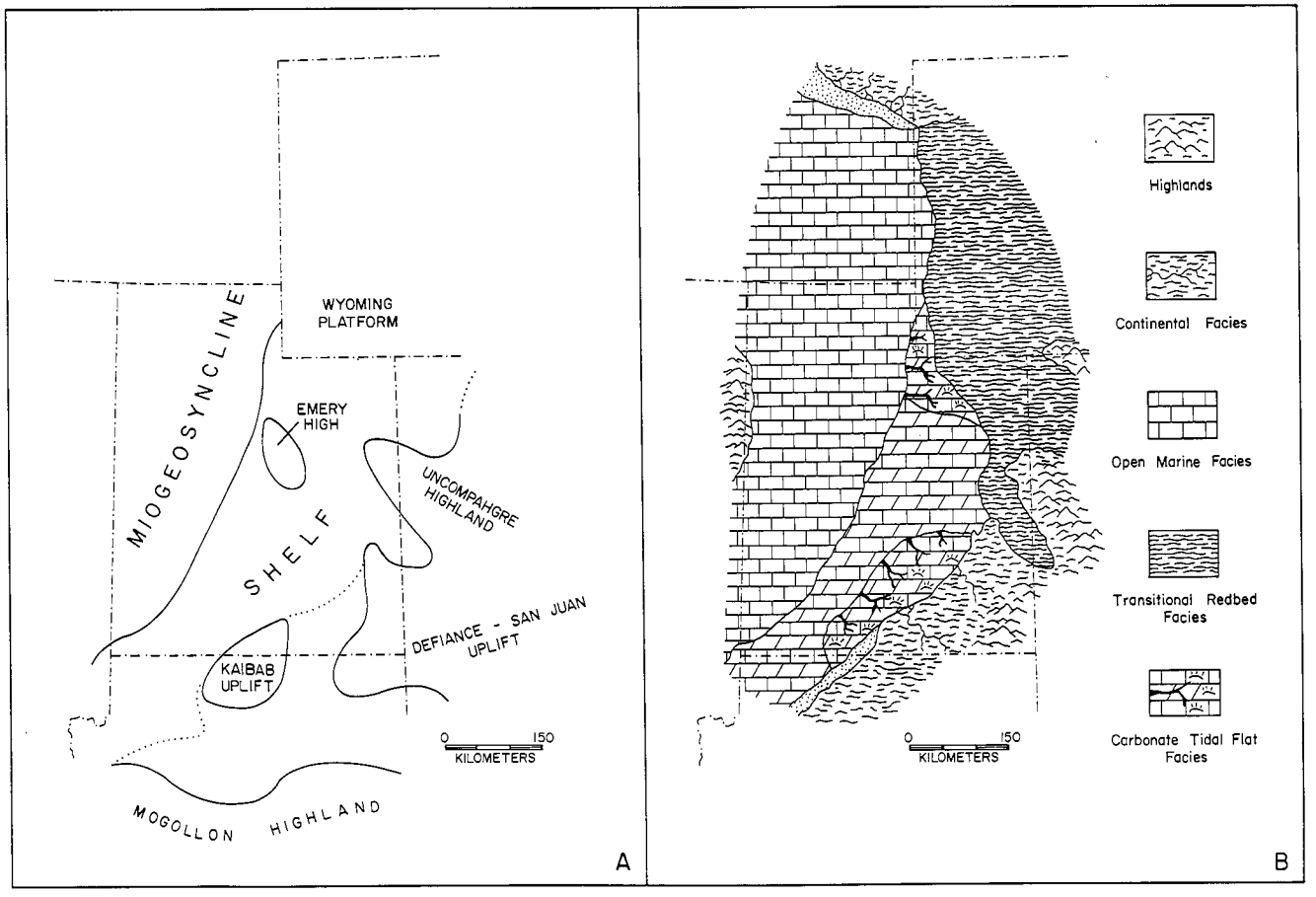

FIGURE 6.–A.–Paleotectonic features affecting deposition in Utah and surrounding states during the Early Triassic. Modified after Blakey (1974). B.–Paleogeography and sedimentary facies during deposition of lithofacies A. Modified after Koch (1976).

derlying Black Dragon Member to pale yellow gray dolomicrite of the basal Sinbad Member. In the Capitol Wash and Pleasant Creek sections this basal contact is marked by a thick zone of vertical interfingering between the two members, with as much as 1.3 m of Black Dragon redbeds occurring 4 m up into the Sinbad carbonates. Contacts between the two members are largely gradational. In sections which lack the interfingering, a transition zone of from several centimeters to several meters exists. Local scour-and-fill contacts in some southern sections were almost certainly produced by tidal channels cutting down through lower gradational beds.

Mineralogically, lithofacies A consists mainly of dolomite, with less than 20 percent calcite, gypsum, pyrite, hematite, limonite, and terrigenous clastics–mainly quartz, muscovite, and clay minerals.

Five petrographically separate, but genetically related, subfacies are defined in lithofacies A; they are the stromatolitic boundstone subfacies, oolite-peloid packstone subfacies, dolomicritic subfacies, channel conglomerate subfacies, and evaporite subfacies.

Stromatolitic Boundstone Subfacies

The stromatolitic boundstone subfacies comprises up to 30 percent of lithofacies A in northern and western sections, but occurs sporadically to the south. These kinds of rocks are absent in the South Draw section. The subfacies is typically medium to massive bedded, forming prominent ledges and cliffs up to 2.0 m thick, and is usually limited to the lower third of the lithofacies, except in the Chimney Rock section where cyclically bedded boundstones are found up to lithofacies B.

Petrographically, the subfacies is characterized by an irregular to laminoid fenestral fabric of grain-supported and relatively undeformed pellets, peloids, oolites, and fine silt-size quartz grains in a dolomicritic to hypidiotopic, finely crystalline dolomite cement (fig. 7). Peloids (0.25 mm–several mm) are the most common allochems, followed by locally abundant pellets (0.4–0.6 mm), less common oolites (0.4–0.6 mm), and rare bioclasts. Lithic intraclasts, mainly small curled dolomicrite chips, and larger (up to 2 mm) rip-up clasts are important constituents in some thin sections. Individual fenestrae are both oval (birdseye) and laminar sheetlike cavities which range up to 1 cm long, most being 2–5 mm. Most fenestrae are filled with a coarse mosaic to drusy spar and less commonly with geopetal accumulations of dolomicrite (fig. 7).

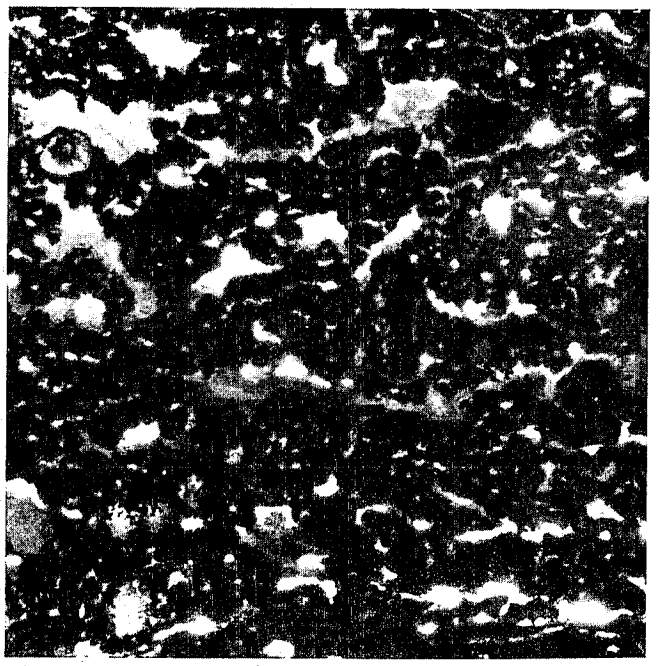

FIGURE 7.–Photomicrograph from unit 16 of the Miners Mountain section showing irregular to laminoid fenestral fabric of stromatolitic boundstone containing mostly peloidal intraclasts. Individual fenestrae are floored with geopetal accumulations of dolomicrite, X10.

Several thin sections show thin, discontinuous lenses of dolomicrite laced with fine quartz silt and possible dolomite rhombs interlaminated with the boundstone. Iron-stained filamentous laminae were occasionally observed and represent possible remains of the original trapping algae.

Morphologically, stromatolites within this subfacies correspond to the LLH and LLH-S type (Logan and others 1964) and consist of crinkly to undulatory, continuous laminae with occasional laterally linked hemispheroids (cabbage heads). Figure 8 shows cryptalgal dolomicrite grading up into "spongy" irregular, fenestral boundstone, capped by cabbage-head stromatolites from lowermost beds of the Chimney Rock section.

No whole fossils were found in the stromatolitic boundstone subfacies, but broken and abraded mollusk fragments, some silicified, were occasionally seen incorporated into the algal-mat structure with other poorly sorted allochems. No extensive bioturbation was observed in any boundstone rocks, and even vertical *Skolithos*-type burrows are rare.

Sedimentary structures indicative of sediment transport were neither expected nor seen in the boundstone subfacies but desiccation features and "tepee structures" are locally common in most measured sections. Probable sheet cracks (parallel to bedding) were observed in rocks with laminoid-type fenestrae and are characterized by collapse and rotation of the impinging fenestral roof. Prism cracks are much more common and noted in both the laminoid and irregular fenestral fabrics. These cracks, up to several cm deep, are marked by several laminae, bound by vertical fractures, which have bowed to become concave upward. Broken pieces of underlying arched laminae were commonly incorporated into the overlying layers of dolomicrite with little evidence of their having been transported from the zone of original desiccation.

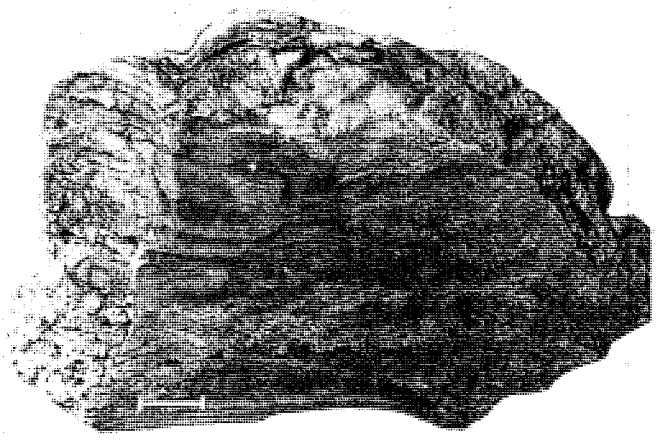

FIGURE 8.–Slab from lithofacies A of the Chimney Rock section showing cryptalgal dolomicrite grading into stromatolitic boundstone and capped by "cabbage-head" hemispheroids. Bar is 5 cm long.

Tepee structures within the subfacies rarely showed elevation of more than 10 cm, but one horizon in the Torrey section shows several arched crests 30 cm high. All such structures show central fractures, and several appear to be complex forms with several generations of cracks superposed on the upturned limbs of main tepees. No evidence of caliche or heterogeneous dolomite formation within central cavities was observed.

Oolite-peloid Packstone Subfacies

The oolite-peloid packstone subfacies, like the stromatolite boundstone subfacies, is more significant to the northwest where it comprises up to 25 percent of lithofacies A. In the southern sections such rocks become thin and discontinuous. Where both the packstone and stromatolitic subfacies occur together, either separated by other rocks or in cycles, the oolite-peloid packstones occur stratigraphically higher than the boundstones and often grade into the more calcareous rocks of lithofacies B. Although petrographically the packstone subfacies shows considerable variation from east to west, it typically forms ledges in thin to medium beds up to 1 m thick.

The Torrey section, in the northwestern part of the study area, yields rocks considerably more calcareous than those observed in other sections with the subfacies characterized there by algal-oolite packstones and wackestones, partly recrystallized, with interstices overprinted by finely crystalline dolomitization (figs. 9, 10). Allochems, generally poorly sorted, are remarkably diverse, and consist mainly of small oolites (0.15–0.25 mm), algal tubes and spheres (up to 5 mm, most 1–2 mm), pellets (0.07–0.12 mm), and peloids (1–3 mm). Bioclasts, showing obvious signs of transportation, are mainly molluscan, but include the only echinoderm fragments found in the lithofacies. Dolomicrite chips are locally important. Microspar (5–30 μ) and pseudospar (>30 μ) form portions of the matrix but unrecrystallized, undolomitized micrite is widely present. Dolomitized matrix makes up to 20 percent in some thin sections, where it is finely crystalline and xenotopic.

Most oolites, but rarely peloids or pellets, also show evidence of neomorphic recrystallization and resulting destruction of their original accretionary texture. Bioclastic fragments and the recrystallized interior of oolites are usually filled with blocky mosaic spar but are occasionally leached.

Eastern and southern sections differ from the Torrey section by their marked decrease in fossil fragments (especially algal tubes and echinoderm debris) and the increase of peloids as principal allochems. In these sections the subfacies is characterized by abundant peloids of two predominant sizes (0.2–0.3 and 0.5–0.7 mm), fewer oolites than in the Torrey section but similar pellets, and a definite increase in lithoclasts (up to 6 mm). Many lithic intraclasts have wispy edges as if they were torn up from a muddy substrate. Bioclasts, exclusively molluscan, never compose more than 10 percent of total allochems. Cementing matrix in these sections is typically dolomicritic or finely crystalline hypidiotopic dolomite. Original intergranular micrite and any neomorphic fabrics have been overprinted and destroyed by dolomitization. Several thin sections exhibit patches of dolomicrite which appear homogeneous but have a clotted fabric with probable peloid ghosts.

Sedimentary structures indicative of current movement are common throughout the Sinbad Member where agitation was sufficient to concentrate oolites and/or peloids as the principal allochems. The oolite-peloid packstone subfacies commonly exhibits ripple bedding, trough and planar cross stratification, small-scale scour structures, and micrograded beds. Typical ripple laminae have foreset bundles 1–3 cm high and are capped by straight-crested oscillation or less commonly undulatory sublingoid ripples with amplitudes from 0.8–2.5 cm and wavelengths up to 15 cm. Low-angle cross stratification without ripple crests occurs in sets up to 7 cm high and 30 cm long and appears unidirectional. Current direction determination was complicated by the ledge-forming nature of most units and limited bedding-plane exposures, but transportation trends are consistently to the southwest, west, and northwest with bidirectional oscillation generally northwest-southeast.

No whole fossils were recovered from the subfacies, but abraded fragments of bivalves, gastropods, calcareous algae, and occasional echinoderms were observed in thin sections. Bioturbation is not intense, but locally *Skolithos* and *Arenocolites* burrows are common.

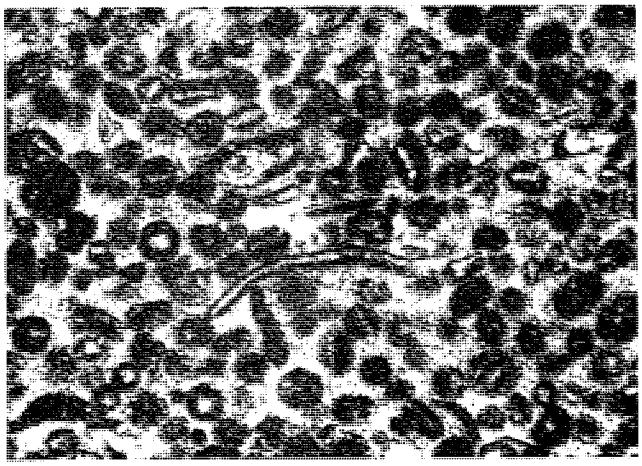

FIGURE 9.—Photomicrograph showing recrystallized packstone fabric of oolites and peloids from upper lithofacies A, unit 18, Torrey section, X37.5.

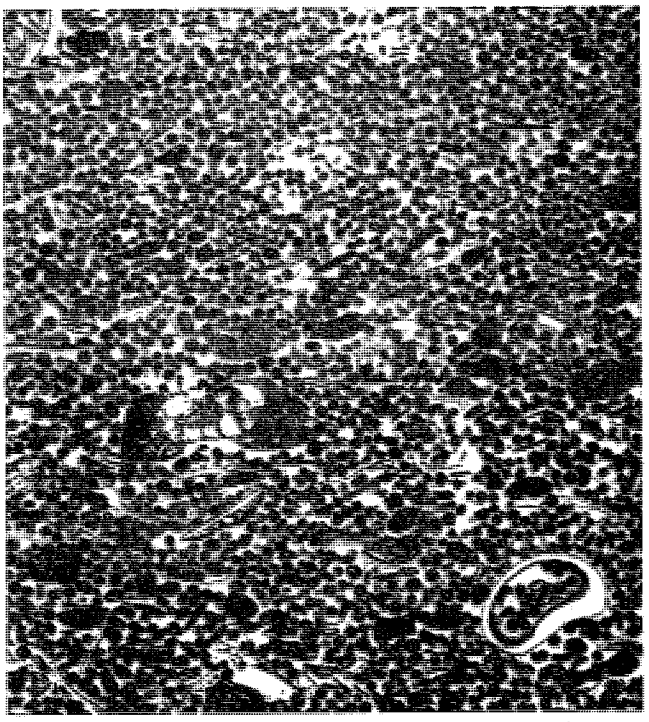

FIGURE 10. Photomicrograph of packstone similar to figure 9 but lacking pervasive recrystallization, unit 20, Torrey section, X10.7.

Dolomicrite Subfacies

The dolomicrite subfacies makes up from 10–60 percent of lithofacies A where these rocks occur as poorly indurated, ledgy-slope-forming beds up to 0.5 m thick. The subfacies is characterized by a uniform lithology expressed in several distinct bedding styles, mainly cryptalgal, massive, and rippled.

Petrographically the subfacies consists of aphanocrystalline dolomicrite, with up to 35 percent finely crystalline hypidiotopic dolomite in microlenses or dispersed equantly throughout the matrix. Relict peloidal fabric is occasionally preserved as a patchy background fabric, but small dense pellets (0.5–0.8 mm) remain unaltered.

The cryptalgal dolomicrite is dense, lacks fenestrae or textural voids of any kind, but exhibits probable algal-controlled crinkly and wavy laminae, often layered contrary to gravity. Figure 11 shows typical cryptalgal dolomicrite arched over a lag of whole gastropods, which have been recrystallized and partly filled with dolomicritic mud.

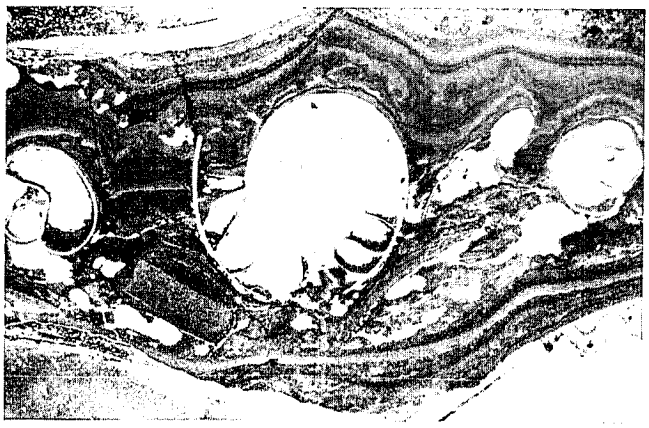

FIGURE 11. Photomicrograph showing cryptalgal dolomicrite arched over mollusk storm lag from unit 20, Chimney Rock section, X10.

The massive dolomicrite, often found in the transition zone as the first Sinbad unit above the Black Dragon Member, is featureless. Allochems and sedimentary structures are generally lacking, but etching and weathered surfaces occasionally reveal a faint lamination which appears to be due to a minor variation in clay or fine silt. Massive dolomicrite often covers stromatolitic boundstone with a remarkably sharp contact, as if the algal mat was inundated by a rapid influx of mud.

All dolomicrite not included in the crinkly bedded cryptalgal or structureless massive varieties is referred to as rippled dolomicrite. As the name implies, it is typically ripple bedded and may contain thin claystone laminae. Rippled dolomicrite contains considerably more finely crystalline dolomite, very fine quartz silt, and scattered euhedral dolorhombs (<0.1 mm) than either of the other varieties. Dolomicrite chiplike rip-up clasts are locally abundant, sufficient for some rocks to be classified as lithoclastic wackestones.

Virtually all sedimentary structures in the subfacies are limited to the rippled dolomicrites and consist mainly of straight-crested and sublingoid ripples with low-angle ripple lamination and carbonate flaser bedding. One polished slab (fig. 12A) shows anomalously high-angle planar cross lamination of more than 60° in truncated sets several centimeters high. Straight-crested ripples are generally of the symmetrical oscillation type with amplitudes up to 1.5 cm and wavelengths of 7 cm. Less common current ripples approach sublingoid geometries with amplitudes of 1 cm and wavelengths of 5 cm. Several current ripples have faint interference ripples intersecting them at 90°, producing rhomboid troughs of 7 × 3 cm.

Small-scale ripple troughs of finely crystalline dolomite filled with flasers of dolomicrite (fig. 12B) are herein referred to as carbonate flaser bedding to distinguish them from the sensu-stricto usage of flaser bedding in clastic environments. Carbonate flaser bedding was observed in thin section and from polished slabs and presumably results from the same process of agitation involving two separate grain sizes that produces shale-in-sand flaser bedding.

Current direction was west-northwest, with oscillation back to the east and southeast. Interference patterns indicate a northeast to north-south secondary current was also present.

The only whole fossils observed in the subfacies are scattered high-spired gastropods, mostly well sorted and found in discrete lags. Abraded bioclasts are generally sparse, are always molluscan, and account for no more than 5 percent of the total sample. Bioturbation within the dolomicrite subfacies is sporadic and dominated by vertical *Skolithos* burrows with rare horizontal feeding traces. Several beds of mottled dolomicrite with obviously disturbed bedding are thought to represent total bioturbation although no individual burrows or traces were found.

Channel Conglomerate Subfacies

The channel conglomerate subfacies comprises from 2–10 percent of lithofacies A and occurs in discontinuous lenses and channels up to 0.5 m thick throughout the study area. Poor sorting characterizes most samples which contain lithic intraclasts up to 20 cm long in a matrix of smaller sand- and gravel-sized clasts, oolites, pelloids, and silicified bioclasts (figs. 12C and 13). All lithic clasts are identifiable as having been derived from lithofacies A and are cemented in a fine to medium crystalline, hypidiotopic to idiotopic dolomite cement. Clastic quartz grains and mica flakes are locally abundant.

Two varieties of conglomerates were observed, those with flat pebbles (edgewise) and those with predominantly subrounded to subangular clasts. Although not mutually exclusive, where flat-pebble conglomerates dominate, the coarseness of the matrix and crystal size of the cement is less. Flat-pebble conglomerates are more loosely packed and occur with greater regularity in the northern sections. The tighter packed, subrounded conglomerates are mostly found south of the Grand Wash section.

Bioclasts were not seen and are thus unimportant constituents of the subfacies. No bioturbation of any kind was observed.

No sedimentary structures to indicate current direction were found, but ripple bedding was observed in the upper, moderately sorted portion of one sample. Flat-pebble conglomerates have pebbles oriented with long axes subparallel to bedding, but analysis of pebble imbrication showed variable orientations. Pebbles of this subfacies were obviously transported, in contrast to similar-looking rocks of lithofacies E which are believed to have formed essentially in situ.

Evaporite Subfacies

In the Grand Wash section and to the south, poorly exposed beds of gypsiferous dolomicrite, up to 0.6 m thick, occur with bands (5–20 cm) of small gypsum nodules (fig. 14). Farther south, in the South Draw section this evaporate subfacies is expressed as a single 0.75-m-thick bed of massive gypsum (fig. 15F).

In all northern sections that show this subfacies, it is characterized by featureless, pale yellow dolomicrite laced with dis-

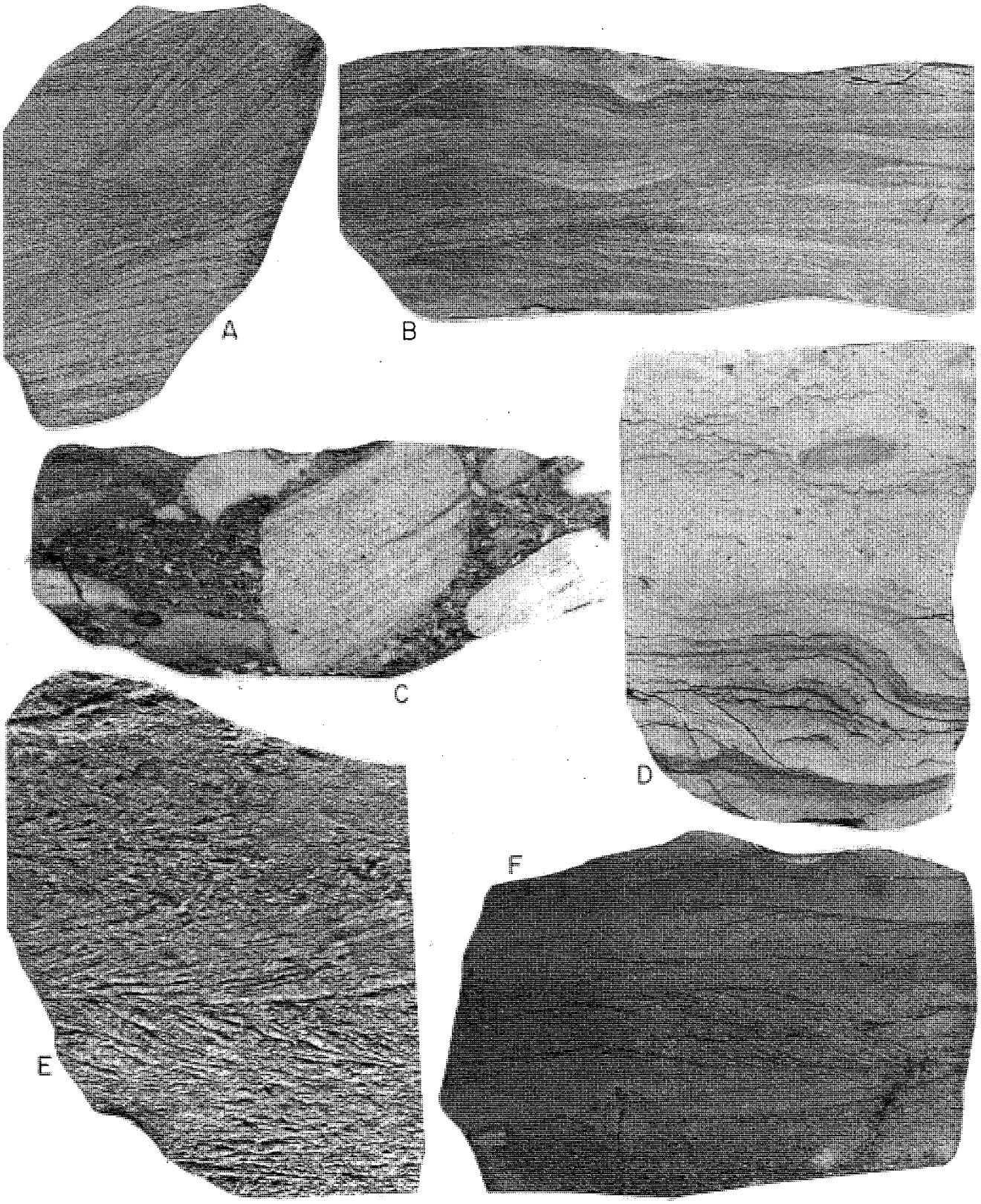

FIGURE 12.–A.–High-angle cross-bedding from dolomicrite subfacies, Cuts Canyon section, X1. B.–Carbonate flaser bedding from dolomicrite subfacies, Chimney Rock section, X1. C.–Channel conglomerate from unit 5, South Draw section, X1. D.–Cryptalgal dolomicrite grading into bioturbated lithoclastic wackestone from unit 19, Grand Wash section, X1. E.–Herringbone cross-bedding in grainstones from upper ledge of lithofacies E, unit 44, Torrey section, X1. F.–Herringbone cross-sets in lens from claystones of lithofacies F, unit 28, South Draw section, X1.

FIGURE 13.–Cryptalgal dolomicrite overlain by lens of channel conglomerate showing both flat-pebble and subrounded intraclasts, lithofacies A, Fremont River section, X1.

tinct oval nodules of light gray gypsum 0.35–2.0 cm long. The gypsum occurs in aggregates of fibrous to bladed crystals (0.05–0.2 mm), which is a form more typical of authigenic anhydrite, suggesting the gypsum is pseudomorphic. Surface exposures are commonly leached, leaving layers of conspicuous oval vugs.

In the South Draw section the discrete nodules are replaced by one massive bed of contorted, ptygmatic gypsum. Dolomicrite, now less than 10 percent, occurs as floating blebs and fractured, wispy laminae that show evidence of replacement by the surrounding gypsum (fig. 16). The gypsum displays an equant, microcrystalline fabric with no remnant of original nodular coalescence or bedding. The contorted nature of the present bedding is probably a response to load variation or tectonic stresses involved in formation of the Teasdale uplift.

No trace of fossil fragments or bioturbation was observed in the subfacies, and sedimentary structures are limited to occasional bedding laminae in the dolomicrite.

FIGURE 14.–Rippled dolomicrite overlain by gypsiferous dolomicrite with oval gypsum nodules from unit 14, Grand Wash section. Bar is 50 cm long.

Lithofacies B

The lowest skeletal-supported limestones and dolomitic limestones encountered in the Sinbad Member mark the base of lithofacies B. The facies is up to 13 m thick in the western sections, near the town of Torrey, but thins eastward to 4 m in the Monas Falls section, and southward to less than 3 m in the South Draw section (fig. 3). Lithofacies B is generally a cliff former, and was observed to have both a disconformable and gradational contact with the bounding dolomites of lithofacies A and C.

Mineralogically, the lithofacies is predominantly calcite in the northern and western sections, where the only true limestone units are found, but follows the general trend of most Sinbad facies and shows increased amount and degree of dolomitization toward the southeast. Dolomite, in finely crystalline cement and rare euhedral dolorhombs, is the next most common mineral. Limonite and hematite (after pyrite) are common as stains and grain coatings in the most bioturbated units, while terrigeneous quartz grains and mica flakes rarely compose more than 5 percent of most samples. Devolatized hydrocarbons, present as stains and void fillings, are abundant and impart a marked petroliferous odor to freshly broken samples. This dead oil is responsible for the medium to dark gray discoloration of most limestone units and serves to highlight saturated allochems and stylolites in thin section and handsample (fig. 17).

Lithofacies B is conveniently divided into two subfacies, a skeletal packstone subfacies and a more limited pelletal wackestone subfacies, both of which may show intense cyclic bioturbation. This bioturbation, combined with the less diverse biota, distinguishes the older limestones of lithofacies B from the younger limestones of lithofacies D.

Skeletal Packstone Subfacies

The skeletal packstone subfacies comprises 70–100 percent of lithofacies B in the various measured sections. It is characterized by grain-supported skeletal allochems of varied sorting, with smaller numbers of pellets (0.1–0.12 mm), oolites, peloids, and micrite lumps. Skeletal material is dominated by bivalves and gastropods (fig. 18) that are usually disarticulated and show signs of abrasion and occasional coating. Echinoderm plates, spines, and rare columnals, and assorted codiacean algal debris make up the remaining skeletal grains. One possible scaphopod and several ostracodes were observed in thin section.

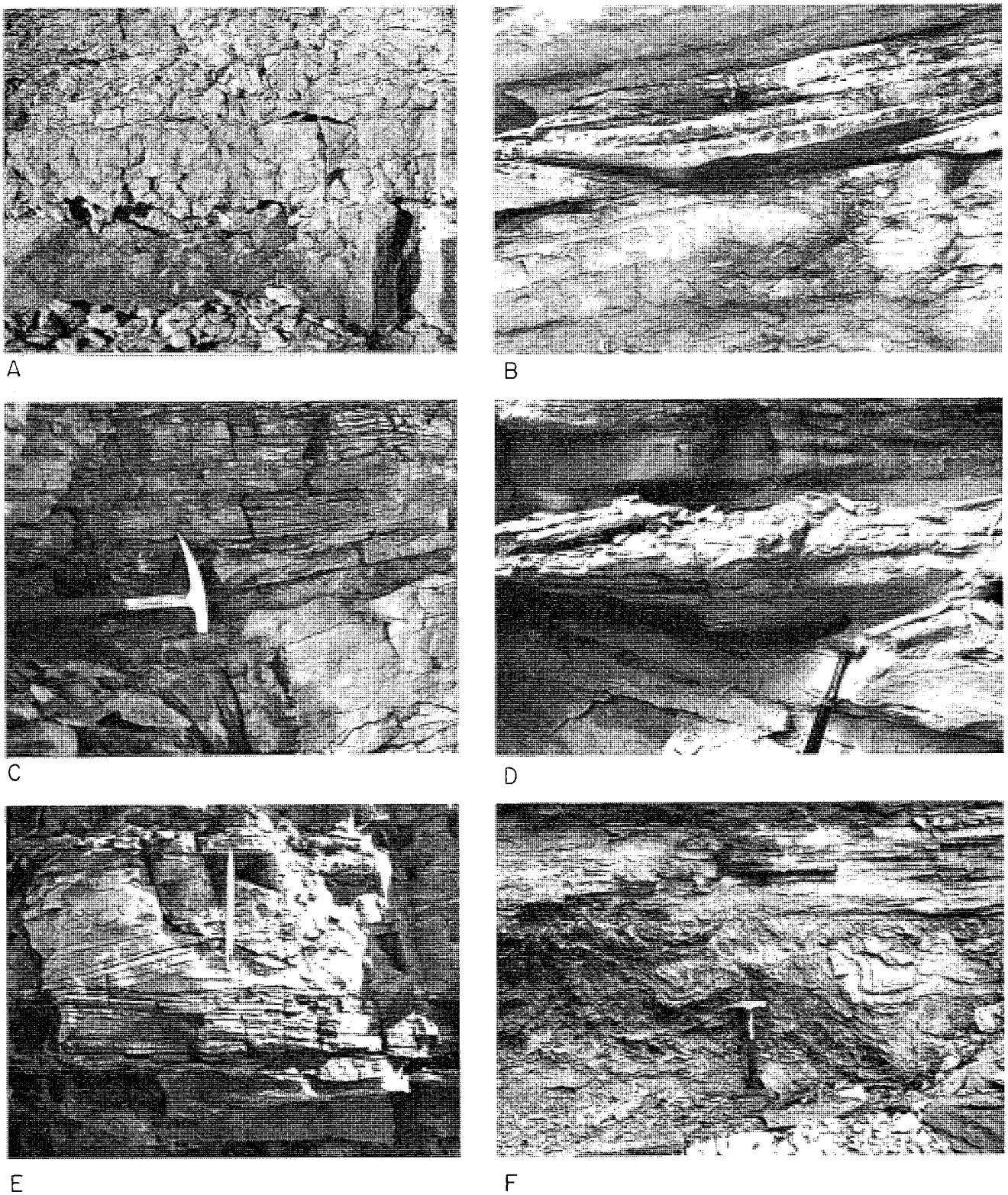

FIGURE 15.–A.–Cyclic bioturbation typical of lithofacies B, showing lower grainstone ledge overlain by increasingly bioturbated wackestones which are generally mottled and crumbly, from unit 32, Torrey section. Bar is 50 cm long. B.–Tidal channel from lithofacies C, unit 24, Capitol Wash section. C.–Skeletal packstone with rippled upper contact overlain by oolitic grainstones of lithofacies D, units 26–27, Pleasant Creek section. D.–Tidal channel characteristic of lithofacies C, Fremont River section. E.–Planar cross-bedding in pelletal wackestone subfacies of lithofacies B, unit 26, Torrey section. F.–Massive bed of ptygmatic gypsum overlain by laminate dolomicrite, units 1–2, South Draw section.

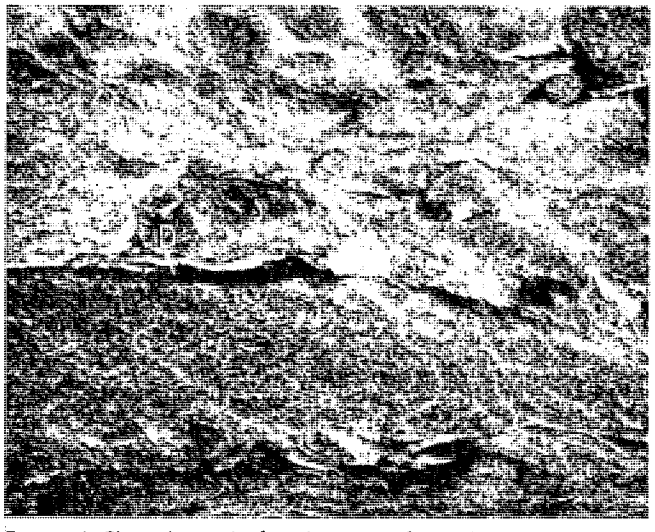

FIGURE 16.–Photomicrograph of massive gypsum from unit 1, South Draw section showing dolomicrite laminae (D) scattered throughout gypsum matrix (G), X8.2.

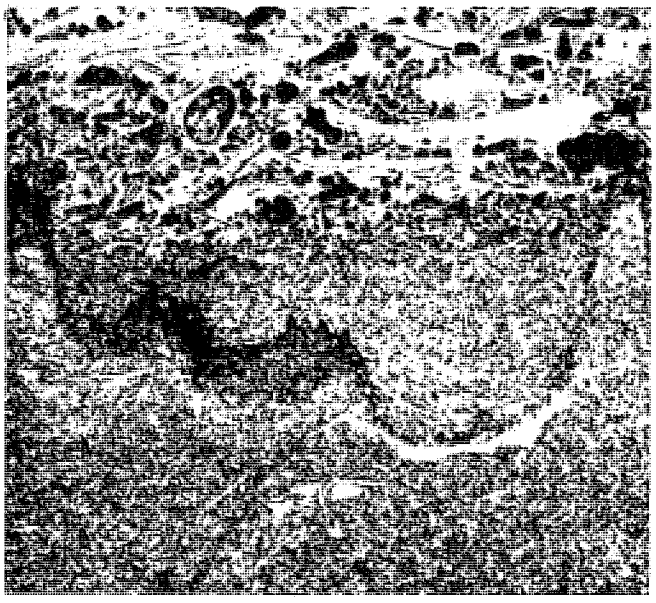

FIGURE 17.–Photomicrograph of pelletal wackestone of lithofacies B overlain by storm-surge grainstone from unit 27, Torrey section. Note oil-soaked stylolite, X10.

Most of the samples analyzed were originally packstones, but interstices are now just as commonly filled with microspar as with micrite. Neomorphic fabrics give way to xenotopic dolomite or dolomicrite in southern sections.

Spar-cemented grainstones are present only in storm-surge layers which form porous bands up to 6 cm thick (fig. 17). These grainstones contain a larger, different suite of bioclasts that are disarticulated and broken. Grainstone cement is usually coarse mosaic spar, but drusy needle fiber spar is common in partially leached, fossil moldic voids. Epitaxial cement was not seen on echinoderm fragments or elsewhere. Most bivalve and gastropod fragments are badly recrystallized and occasionally leached. Bivalve shells show different recrystallization with the inner layer altered to blocky spar and the outer layer still composed of calcite prisms stacked normal to the wall.

FIGURE 18.–Photomicrograph of grainstone layer from figure 17 showing abraded mollusk, algal, and echinoderm bioclasts with oil-stained peloids, X50.

Skeletal grains in packstones are unsorted and poorly washed, and mud, pellets, and abraded shell debris commonly fill chambers of gastropods. Two notable exceptions are well-sorted, selectively dolomitized oolites from the Miners Mountain section, and a well-sorted and washed gastropod coquina from Capitol Wash. Geopetal umbrella structures are not uncommon in packstones, as evidenced by large pelecypod valves shielding underlying areas from infiltrating mud, areas which were later filled with secondary spar (fig. 19).

FIGURE 19.–Photomicrograph showing umbrella structure in wackestone where pelecypod valves shielded underlying voids from mud infiltration. Secondary spar in such areas is commonly leached leaving shelter porosity, unit 19, Capitol Wash section, X38.5.

Stylolites, although not so common as in lithofacies D, are present in several sections of the subfacies and are often accentuated by surface weathering into gaping recesses. Stylolites are generally of the serrate variety and show dissolution columns of several mm. Figure 17 shows the interpenetration along an oil-soaked stylolite of a pelletal packstone into a storm-surge skeletal grainstone. Bleeding of oil from the stylolite into the surrounding matrix is visible.

One of the most characteristic features of both subfacies in lithofacies B is their affinity for intense, often cyclic bioturbation. A typical cycle consists of a basal storm-surge grainstone, overlain by an increasingly pellet-rich packstone with prominent *Skolithos* burrows, and capped by up to a meter of severely bioturbated packstone or wackestone which is increasingly dolomitic. Figure 15A shows a cycle in outcrop from the lower grainstone ledge up to the crumbly, mottled zone of maximum bioturbation. A thin section from the middle of the cycle (fig. 20) shows vertical burrows and the resultant disrupted bedding and churned-up nature of the rock.

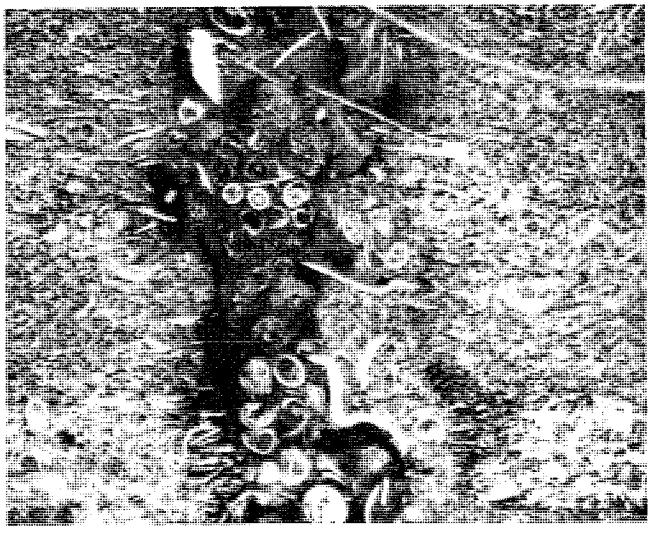

FIGURE 20.—Photomicrograph of *Skolithos* burrow filled with gastropod, algal, and ostracode debris from overlying lagoonal sediments, unit 14, Pleasant Creek section, X41.5.

The skeletal packstone subfacies is a medium to thick and horizontally bedded cliff-former and lacks sedimentary structures other than an occasional rippled surface spared from burrowing. Tepee structures, the only ones observed in lithofacies B, occur at the Monas Falls section where they are fortuitously exposed on a large, bioturbated, bedding plane slab. Individual tepee ridges up to 9 cm high formed on a series of intersecting Triassic fractures which define desiccation polygons several meters wide (fig. 22C).

The apparently contradictory occurrence of tepee structure on bioturbated packstones attests to the local rapid fluctuation betwen subaqueous and subaerial exposure during at least part of the deposition of lithofacies B.

Pelletal Wackestone Subfacies

The pelletal wackestone subfacies forms poorly indurated, gradational interbeds up to 0.4 m thick with the skeletal packstone subfacies. Although thin units of the subfacies are common throughout lithofacies B, the best exposures occur in the Torrey and Pleasant Creek sections. The pelletal wackestone subfacies significantly differs from the skeletal packstone subfacies in the relative paucity (<15 percent) and lack of diversity of skeletal elements, the increase in clastic grains and matrix of dolomitization, and the presence of planar cross-bedding.

Petrographically the subfacies is characterized by abundant dark, dense pellets (0.09–0.11 mm) and locally important peloids (0.25–0.4 mm) in a recrystallized and dolomitized micritic matrix (fig. 20). Neomorphic pseudospar dominates over microspar, and most thin sections contain cloudy patches of remnant micrite. Dolomicrite to medium crystalline hypidiotopic dolomite with isolated euhedral dolohombs may compose up to 35 percent of some samples. Fine silt-size subangular quartz grains and less commonly mica flakes are often significant matrix constituents. Bedding laminations are apparently due to relative increases in these detrital grains.

No whole fossils were recovered from the subfacies, and the few observed molluscan bioclasts (fig. 21) are badly recrystallized. Bioturbation is locally intense but less extensive than in the skeletal packstones, as evidenced by preservation of sedimentary structures.

FIGURE 21.—Photomicrograph of mollusk wackestone from lithofacies D with several microfractures and dissolution surfaces filled with oil, unit 41, Monas Falls section, X8.5.

Planar cross-bedding, in sets up to 12 cm high, is the diagnostic field characteristic of the pelletal wackestone subfacies, for such bedding is especially prominent on weathered subfacies (fig. 15E). Ripple bedding was also observed. Current directions indicate components of sediment transport to the northwest and to the southwest.

Lithofacies C

Lithofacies C averages less than 2 m thick and is the most uniform and petrographically homogeneous rock body in the study area. It ranges from 2.2 m thick in the Torrey section to 0.9 m thick in the South Draw section. The lenticular bedded dolomite of lithofacies C forms a conspicuous recessive break between the cliff-forming limestones of lithofacies B and D (fig. 22E).

Mineralogically, lithofacies C is dominated by dolomite. Terrigenous clastics, as quartz grains, comprise up to 15 percent of some samples, but calcite is relatively unimportant.

Petrographically the lithofacies is characterized by a hypidiotopic fabric of fine to medium crystalline dolomite with lesser amounts of interstitial dolomicrite (fig. 23). Allochems are virtually absent except for rare pellets somehow spared from dolomitization. Several thin sections show what appears to be a relict peloidal fabric that is strongly overprinted by dolomitization and discernible only by the selective nucleation of dolomite crystals.

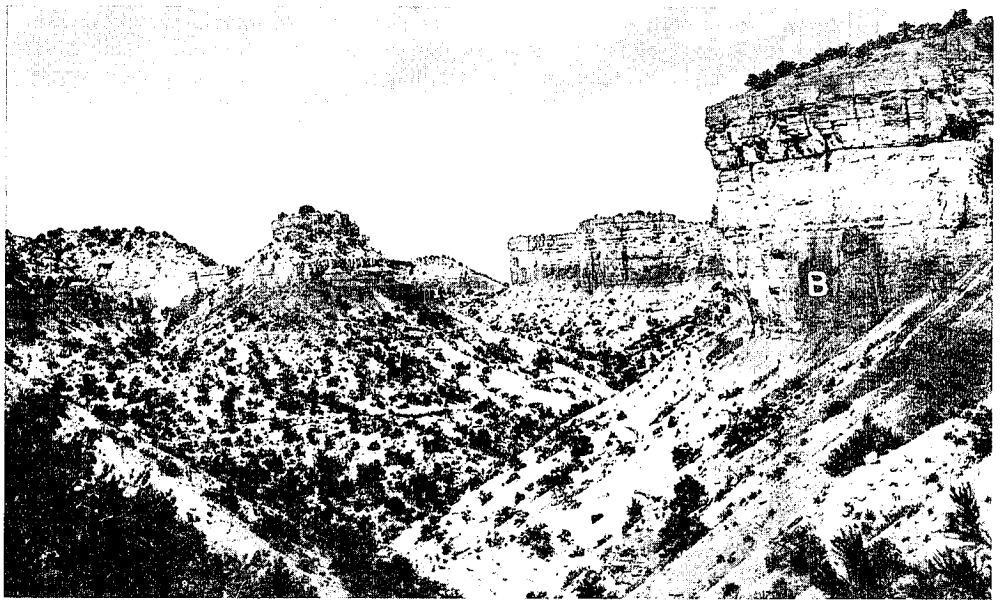

A

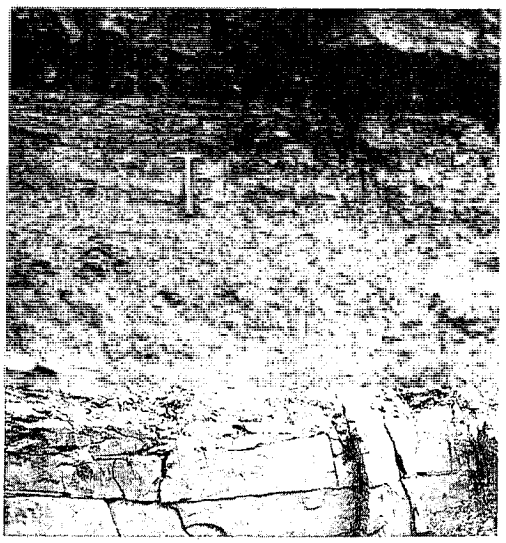

B

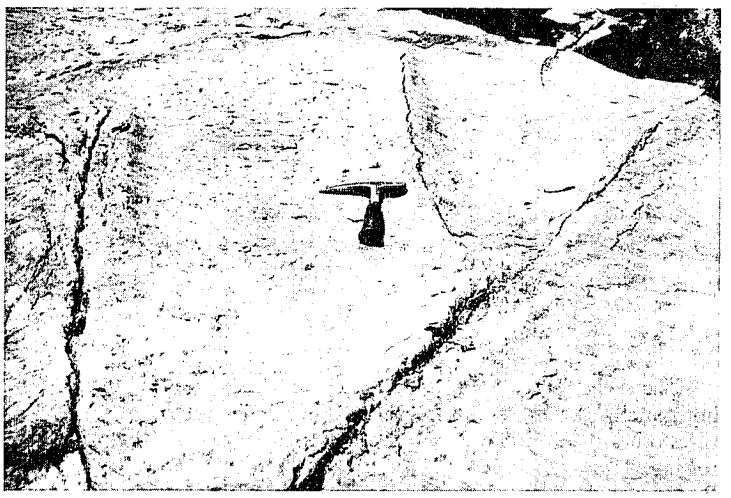

C

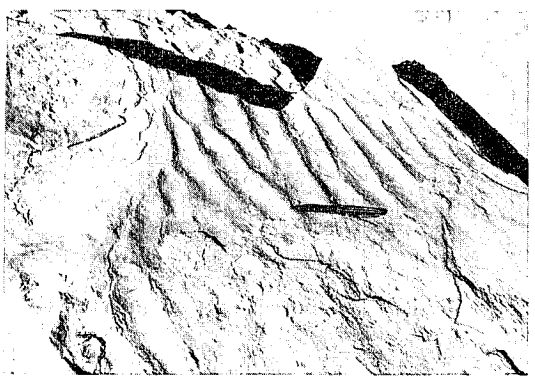

D

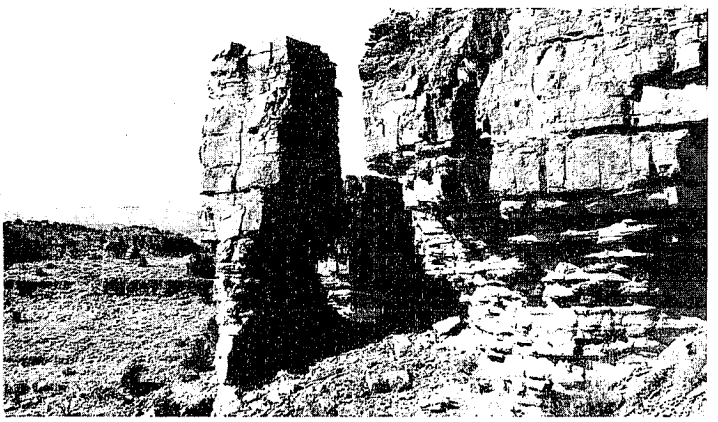

E

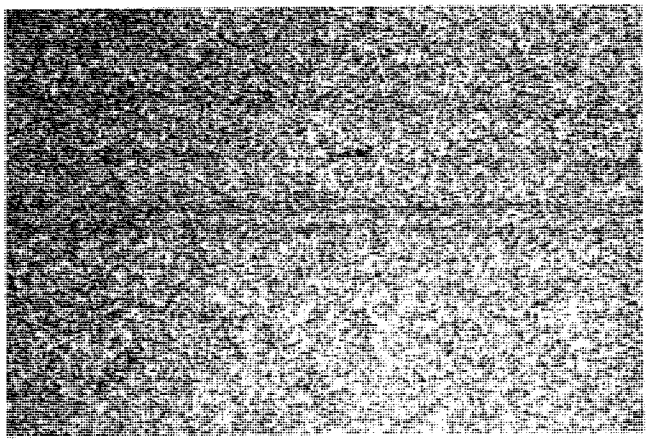

FIGURE 23.–Photomicrograph showing remnant lamination in fabric of finely crystalline, equant dolomite of lithofacies C, unit 28, Grand Wash section, X7.5.

No fossils were recovered from lithofacies C, and bioclastic debris in general is lacking. Bioturbation, however, is prominent and yielded the most diverse ichnofossils observed in the Sinbad Limestone Member. Complete disruptive bioturbation is rare, most units being dominated by several kinds of vertical burrows and a remarkable variety of horizontal feeding trails ranging from millimeters to 3 cm wide (plate 2, figs. 1, 3).

Channeling and low- to medium-angle planar cross-bedding are the most persistent sedimentary structures in the lithofacies. Most channels range from 0.25–2.0 m wide and 0.25–0.5 m deep, imparting a characteristic lenticular bedding to outcrops (fig. 15B). Channel lenses are planar cross-bedded and often show rippled bottoms. Festoon cross-bed sets up to 30 cm high and asymmetrical current ripples between channels were also observed. Current direction, as indicated by sedimentary structures and long axis orientation of channels, was generally toward the west but showed considerable variation which can probably be attributed to overlapping channel geometries and meandering.

Lithofacies D

The prominent upper gray cliffs of the Sinbad Member in the Teasdale Dome are held up by limestone and dolomitic limestone of lithofacies D (fig. 22E). The lithofacies exhibits considerable petrographic variation, laterally, but maintains a fairly constant thickness of 3–4 m throughout the study area. The base of lithofacies D is defined at the abrupt disconformable contact between the finely crystalline dolomite of lithofacies C and the first predominantly calcareous unit above, which is usually skeletal and heavily burrowed. The upper contact with lithofacies E is much less precise, especially in sections south of Miners Mountain, owing to dolomitization and interfingering. For consistency in measuring and correlation, the upper contact of lithofacies D is placed at the youngest occurrence of a grain-supported, predominantly skeletal fabric. For orientation in the field, this upper packstone or grainstone occurs as a medium gray, meringue-weathering bed, 30–40 cm thick, which caps the cliff beneath the lower slopes of lithofacies E.

Mineralogically, lithofacies D is approximately 65 percent calcite and 30 percent dolomite. This 2–1 ratio increases in favor of calcite in northern and western sections, while dolomite becomes more important to the south. Scattered quartz grains and pyrite with alteration rims of iron oxides make up the remaining 5 percent.

Two distinct subfacies were observed in the lithofacies, an oolite-mollusk packstone subfacies, and a peloidal mudstone-wackestone subfacies. A dolomitized grainstone subfacies was observed in an interfingering relationship and will be discussed with lithofacies E.

Oolite-mollusk Packstone Subfacies

The oolite-mollusk packstone subfacies makes up 70 percent of lithofacies D, and comprises the upper and lower third of the cliff, both above and below the peloidal mudstone-wackestone subfacies. Although usually medium to thick and horizontally bedded, the better sorted, more oolitic portions may exhibit low-angle cross-stratification.

Petrographically, the subfacies appears superficially similar to the skeletal subfacies of lithofacies B, but closer analysis reveals subtle and important differences. Allochems in the younger rocks are grain supported, despite local "floating" due to recrystallization, and still consist mainly of bivalve and gastropod fragments. Algal tubes and spheres are noticeably absent, but echinoderm fragments are more numerous and variable. Skeletal allochems are still in the majority, but percentages vary greatly from slide to slide. Nonskeletal grains show greater percentages of oolites, greatly decreased pellets and micrite lumps, but remain the same in peloids. Sorting appears haphazard and varies within centimeters, but most beds are poorly sorted with fragments broken and abraded. Disarticulation of bivalves remains the rule, but exceptions were noted in the northern sections where whole clusters of pelecypods were found with valves intact. Most gastropods are filled with mud (often unrecrystallized) or dark oil-stained pellets (fig. 24). Virtually all skeletal fragments have been recrystallized into a sparry mosaic or, less commonly, into megacrystalline spar showing prominent cleavage. Oolites are commonly recrystallized with some subsequent leaching, but peloids appear unaltered.

FIGURE 24.–Photomicrograph of recrystallized skeletal packstone showing a geopetal-floored gastropod chamber with upper margin leached of spar from lithofacies D, unit 38, Monas Falls section, X38.5.

FIGURE 22.–A.–View of the Grand Wash section, looking west, with Permian Kaibab Limestone (P) exposed in lower slopes and Sinbad Limestone Member (S) forming cliffs along skyline. Redbeds of the Black Dragon Member (B) separate the two carbonate sequences. B.–Hammer is at the contact between crumbly claystones of lithofacies F and overlying silty shales of the Torrey Member, Fremont River section. C.–Tepee ridges on bioturbated slab of lithofacies B, unit 34, Monas Falls section. D.–Typical rippled marks of lithofacies C indicating current transport to the northwest, unit 17, Torrey section. E.–Thick-bedded limestones of lithofacies D are held up by channeled dolomites of lithofacies C which usually weather back to form a prominent recess, Torrey section.

Interstitial matrix is both neomorphic microspar and original micrite with minor dolomicrite. Equant pseudospar and fibrous druse are uncommon but where present are more coarsely crystalline than in the lower limestones. Original mud filtering is indicated by common umbrella structure. Dolorhombs, many zoned, fill both skeletal and nonskeletal grains, but matrix rhombs are rare.

Stylolites are widespread in the oolite-mollusk packstone subfacies, with dissolution penetration of up to several centimeters noted in thin sections. Most stylolites parallel bedding with jagged serrate outlines and appear filled with insoluble, silt-size residue (fig. 25). Stylolites were found in homogeneous lithologies but frequently occur along borders between heterogeneous petrographic fabrics. As in lithofacies B, stylolites, as well as matrix and allochems immediately adjacent to them, are moderately to heavily oil stained, indicating stylolites provided effective conduits for hydrocarbon migration.

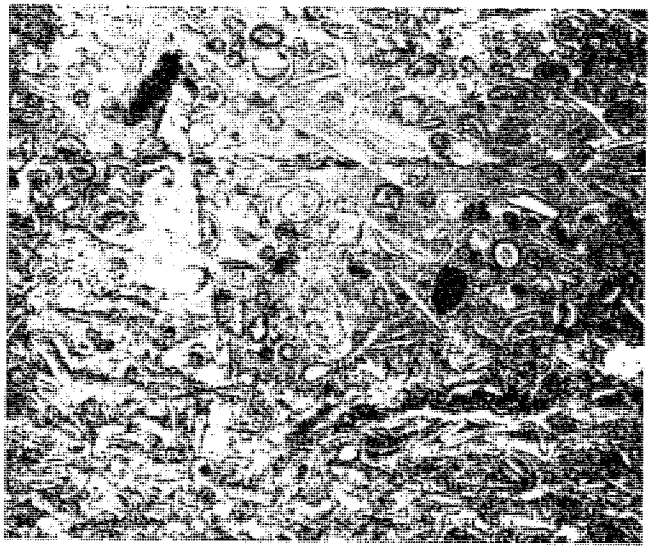

FIGURE 25.–Photomicrograph showing dissolution surface between lower packstone and upper wackestone from unit 41, Monas Falls section. Such stylolites from lithofacies D are typically filled with insoluble residue and are oil stained, X8.4.

Mollusks dominate whole fossils collected from the subfacies, which includes the lowest stratigraphic occurrence of *Meekoceras* sp. Bioturbation, mainly vertical *Skolithos* burrows, is concentrated in "pipe rock" units 10–20 cm thick but never approach the intensity of cyclicity observed in lithofacies B.

Bedding in the subfacies appears uniform and massive, but weathered surfaces often show rippled bedding and low- to medium-angle cross-beds. Coquinoid units are more conducive than those with coated grains to featureless bedding. Figure 15C shows bedding in the subfacies with prominent ripple marks on the top of an otherwise even-bedded dolomitic limestone, overlain by an oolite-rich unit with cross-bedding.

Peloidal Mudstone-wackestone Subfacies

Rocks of the peloidal mudstone-wackestone subfacies make up the remainder of lithofacies D in sections north of and including the Capitol Wash section while the subfacies is replaced in southern sections by interfingering with dolomitized grainstones of lithofacies E. The subfacies always occurs in the middle of the upper cliff and is characterized by light gray homogeneous limestones, which may be slightly dolomitic and are so densely cemented that they display a conchoidal fracture.

Petrographically, all samples have mud-supported matrices with minor microspar and very few distinct allochems, principally nonskeletal. Pellets of the dense, dark variety are the only well-defined allochems and, where locally abundant, give rise to wackestone. Mudstones and wackestones are more commonly composed of vague peloidal clots and small (0.08–0.1 mm), well-sorted, unidentified intraclasts that may be deformed pellets, attenuated parallel to bedding, or squashed micritized bioclasts. Fine silt-size quartz grains are present in minor amounts, but their concentration in thin layers imparts a characteristic lamination to most samples. This lamination is the only sedimentary structure visible in the subfacies.

Whole fossils collected from the subfacies depart from the usual bivalve-gastropod faunas and consist mainly of several genera of ceratite ammonoids and a notable occurrence of a lyssakid sponge. Examples are poorly preserved, but with spicule net largely undisturbed. No bioturbation was observed in the peloidal mudstone-wackestone subfacies.

Lithofacies E

The dolomitized grainstones of lithofacies E comprise the upper slope and blocky-weathering ledge found in all sections above the cliffs of lithofacies D (fig. 26). Although this lithofacies maintains a fairly constant thickness of 5–7 m, these rocks make up less than 14 percent of the 43-m-thick Chimney Rock section, but almost a quarter of the 25-m-thick section at South Draw (fig. 4). Lithofacies E is one of the most carefully studied rock sequences but was not divided into subfacies. Several distinct lithologies are recognized and described, but overprinting of original fabrics by recrystallization and dolomitization has made the spatial occurrence of similar rocks more a function of diagenetic degree than of primary deposition.

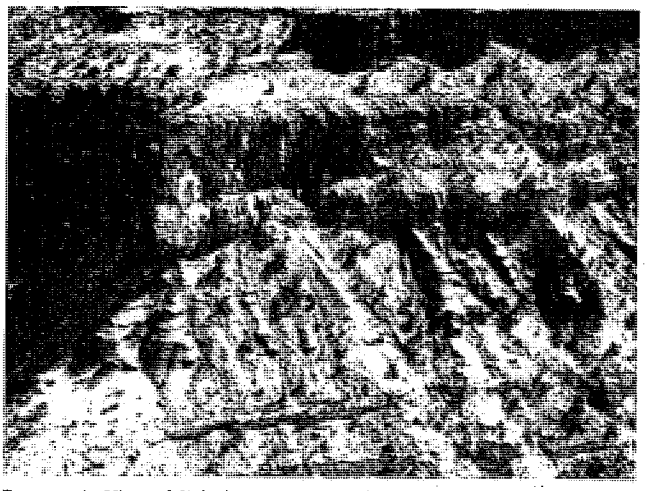

FIGURE 26.–View of Sinbad Limestone Member in Sulphur Creek Gorge just east of Chimney Rock section. All six lithofacies are visible, especially lower slope-forming sequence of lithofacies E.

Mineralogically, dolomite accounts for 80 percent of the lithofacies although various forms of calcite cement are common in the lower beds which grade into and interfinger with lithofacies D. Concretions of limonite after pyrite up to 3.0 cm long are widespread in upper beds, and abundant iron oxide staining imparts an orangish brown tint to several units in outcrop. Clastic grains in southern sections may comprise up to 15 percent of some samples but the "sandstones" of Smith and others (1963, p. 12) owe their texture to coarse euhedral dolorhombs, rather than to quartz sand grains (fig. 27).

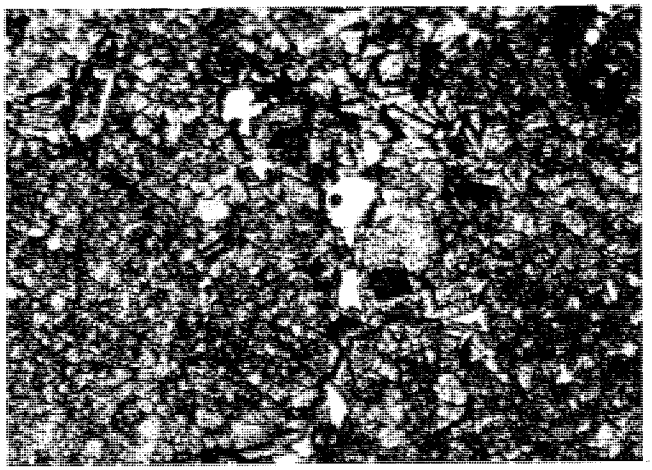

FIGURE 27.—Photomicrograph showing fabric of heterogeneous dolomite of upper lithofacies E, unit 45, Torrey section. Note rapid variation in crystal size of dolorhombs and intercrystalline porosity, X38.5.

Lithofacies E may be conveniently divided into a lower 4–5-m-thick, slope-forming sequence, and an upper 1.5–2.0-m-thick massive ledge. The lowermost beds of the slope-forming unit are petrographically similar to lithofacies D, distinguished by fewer skeletal allochems and increased dolomitization of coated grains (fig. 28). These beds quickly grade vertically into ripple-bedded oolite grainstones that become increasingly dolomitic upward. Well-sorted oolites and peloids (0.25–0.35 mm) make up most allochems, with relatively minor mollusk bioclasts.

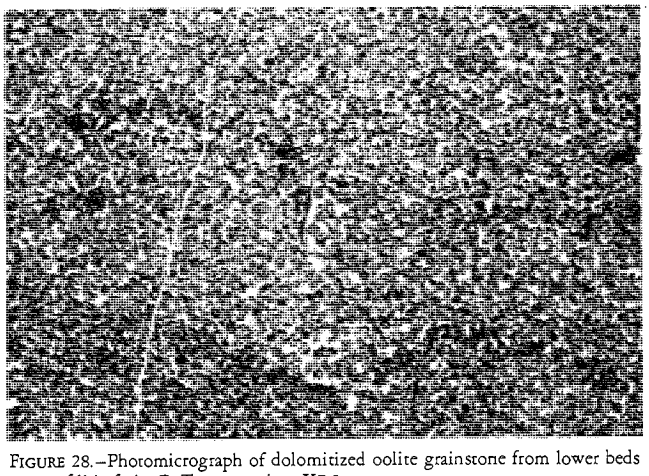

FIGURE 28.—Phoromicrograph of dolomitized oolite grainstone from lower beds of lithofacies E, Torrey section, X7.5.

Oolites generally lack concentric or radial structure because of internal growth of dolorhombs but maintain remnant micrite envelopes (fig. 29). Cementing matrix in lower beds is surprisingly calcitic, in the form of medium crystalline equant spar, but becomes dolomicritic to medium-crystalline idiotopic dolomite upsection and toward the south. Although these rocks are classified as grainstones, differentiation between spar and pseudospar in them is problematical. Cloudy patches of micrite (?), visible in some thin sections, suggest some original fabric was partially packstone.

Large individual dolorhombs (up to 0.3 mm) are restricted to allochems where they usually conform to the confining shape, but occasionally penetrate oolite rims, or burst host grains altogether. Most such rhombs are ankeritic and zoned (fig. 29).

Thin beds of argillaceous dolomicrite and homogeneous finely crystalline dolomite similar to lithofacies C are interbedded with the dolomitized grainstones in the slope sequence. In the southern sections, particularly South Draw and Pleasant Creek, interfingering between these grainstones and the greenish-gray dolomitic claystones of lithofacies F was observed. These interbeds, up to a meter thick, are poorly exposed as float-covered, popcorn-weathering slopes and require trenching to verify their presence.

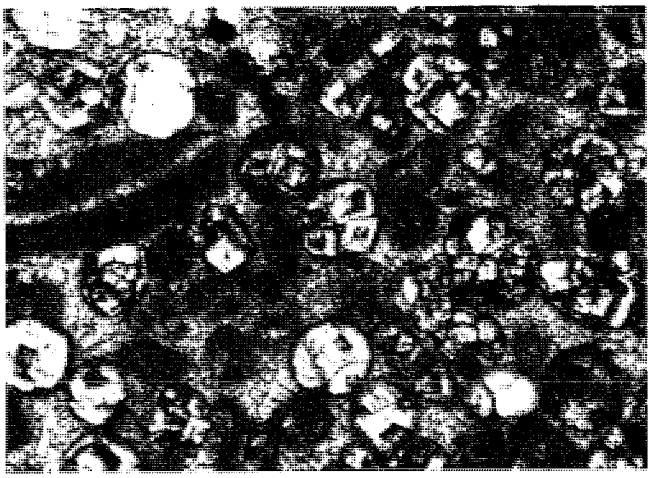

FIGURE 29.—Photomicrograph of dolomite fabric from lower lithofacies E, unit 42, Torrey section showing oolites bursting with euhedral dolorhombs while adjacent peloids are unaltered. Oomoldic porosity is common where dolomite has been leached, X38.5.

The upper ledge-forming beds of lithofacies E exhibit a fascinating variety of dolomite fabrics. In contrast to lower beds, where larger euhedral dolorhombs are limited to selected allochems and finely crystalline dolomite dominates the matrix, the upper more pervasively dolomitized units show dolomicritized allochems and coarsely crystalline interstices (fig. 30). Peloids are increasingly common vertically, but because of the intensity of dolomitization differentiation between oolite and peloid is sometimes not possible. Idiotopic fabrics dominate in these

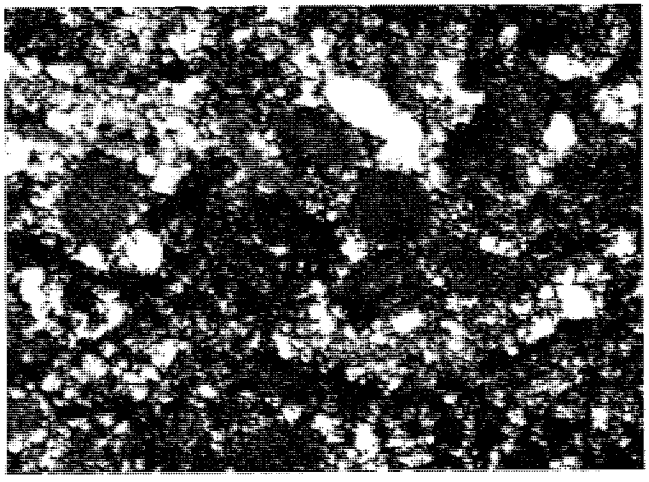

FIGURE 30.—Photomicrograph showing dolomicritized peloids from upper lithofacies E, unit 25, South Draw section, in a medium to coarsely crystalline hypidiotopic dolomite matrix, X38.5.

rocks. Distinct euhedral dolorhombs, many zoned, show poikilotopic penetration of allochems and matrix. Relict fabrics are obvious where finer-grained, dolomitized allochems were apparently spared from later diagenesis, but are subtle in other rocks where original fabric is preserved only as a differential iron coloration of dolorhombs. Dead hydrocarbons ubiquitously fill leached and intercrystalline voids in these rocks, where porosity has obviously been enhanced.

No fossils were preserved in the upper ledge rocks although distinct fossil moldic voids were observed in the Torrey section. Lower slope-forming beds contain large bivalves on bedding planes in the transition zone above lithofacies D. These bivalves, except for minor mollusk bioclasts in thin sections, comprise the only fossils found in the lithofacies. Bioturbation, in the form of vertical burrows and horizontal trails, is only locally important and is restricted to rippled beds.

Asymmetrical current ripples and oscillation ripples are the most prevalent sedimentary structures preserved in the lower sequence and provide accurate directions of sediment transport on the widespread bedding-plane exposures. Two directions were observed, one a northwest-southeast trend and the other a north-south trend. These trends are occasionally superposed in interference patterns but more commonly occur separately.

Herringbone cross-bedding characterizes the upper ledge-forming units in low-angle, tabular sets 2–3 cm high that have upper and lower truncations (fig. 12E). The ledge-forming dolomite is usually massive and laterally continuous but at the Monas Falls section contains a large (2 m deep × 20 m wide) channel cut into the underlying slope-forming beds (fig. 31). The channel strikes roughly east-west and contains coarsely crystalline dolomite with relict grainstone fabric, typical of upper lithofacies E.

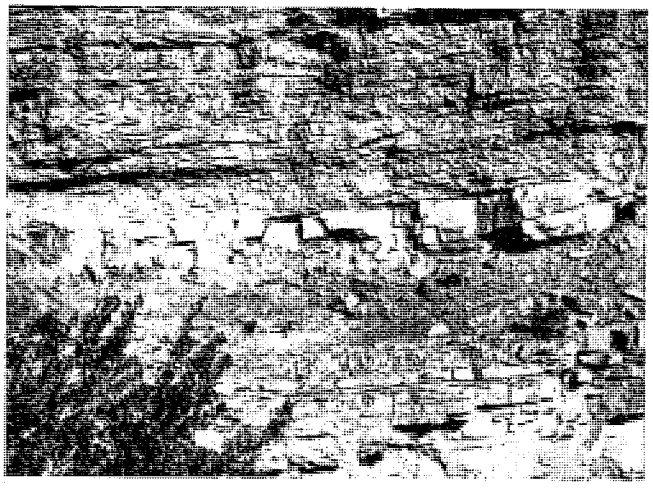

FIGURE 31.—View of tidal channel in upper ledge of lithofacies E, unit 51, Monas Falls section, overlain by claystones of lithofacies F. Channel is oriented roughly east west and is more than 2 m deep.

Thin units of flat-pebble conglomerate are the only other sedimentary structures in the lithofacies and are limited to the South Draw section. Intraclasts are all several centimeters across, layered parallel to bedding, and dolomicritic, in contrast with the coarser crystalline matrix.

Lithofacies F

The greenish gray dolomitic claystones of lithofacies F are the most poorly exposed rocks in the study area. They are easily weathered and are usually stripped off the indurated dolomite of lithofacies E which forms prominent dip slopes along the east flank of the Teasdale Dome. All measured sections show thicknesses of from 1 to 2 m, but most contacts were estimated on float-covered slopes. All sections agree fairly well, however, with reliable measurements of 1.3 and 2.05 m at the better-exposed Fremont River and Monas Falls sections.

The upper boundary of lithofacies F is the contact of the Sinbad Limestone Member with the overlying Torrey Member. Although gradational in most sections, the contact was easily estimated on the basis of an increase in ferric iron coloration, increase in clastic amount and coarseness, and decrease in dolomitic cement. At the better-exposed sections the contact was drawn at the sharp, conspicuous color change between the gray green claystones of lithofacies F and pale reddish brown silty shales of the lower Torrey Member (fig. 22B).

Lithofacies F is predominantly claystone, with minor lenses of dolomicrite and argillaceous peloidal packstone. Expansive disaggregation in water- and popcorn-weathering slopes suggests clays are of the smectite family although detailed analysis was not attempted.

Thin sections reveal a platy to microlaminate structure in most claystones, with peloidal intraclasts showing signs of compressive deformation and elongation. No fossils or bioturbation were observed in any of the measured sections.

Claystone laminae are occasionally rippled with wavelengths from several mm to 5 cm. One sample from the South Draw section exhibits peculiar herringbone cross-lamination (fig. 12F) with peloids anomolously perched one deep on each foreset slope. No evidence of current direction was observed in the field.

Correlation of Lithofacies

Blakey (1974) recognized three facies from the Sinbad Limestone Member in the San Rafael Swell, 40–50 km northeast of the Teasdale Dome study area. He defined a basal skeletal calcarenite; a middle silty, peloidal calcilutite; and an upper dolomitized calcarenite. A fourth facies, a thin sandy dolomite, was recognized in the Circle Cliffs and Orange Cliffs regions.

In the Teasdale Dome area lithofacies B and D of this study are most similar to the skeletal calcarenite of Blakey, but instead of being the basal facies, they are separated from the underlying Black Dragon Member by up to 25 m of dolomite included in lithofacies A. The channeled dolomite of lithofacies C, which separates the two calcareous units, was apparently unrecognized by Blakey. The silty calcilutite does not correlate well with any of the lithofacies defined from the Teasdale area but by virtue of its position probably represents a lateral facies change of the lower slope-forming grainstones of lithofacies E. The upper dolomite of lithofacies E almost certainly correlates with the dolomitized calcarenite facies from the San Rafael Swell. Rocks of lithofacies E, although relatively clastic free in the study area, would logically increase in terrigenous derived clastics to the south and probably correlate with the sandy dolomite facies as well.

The Timpoweap Member, a Sinbad Member equivalent to the southwest, was divided into three general facies by Bahr (1963) as follows: a northwestern "normal marine" facies, a central "platform" facies, and a southeastern "lagoonal" facies. The northwestern facies of predominantly argillaceous and cherty limestones undoubtedly represents a lateral basinward change from the shallow-water carbonates of the study area and lacks a deep-water equivalent in the Teasdale Dome. The central facies contains algal, pelletal, and oolitic limestones with lo-

cal bioherm patch reefs which are occasionally dolomitized. Although still farther out on the platform than the Sinbad beds, these rocks are roughly correlative with lithofacies B and D. The southeastern facies is characterized by finely crystalline, "evaporitic-type" dolomite, red silty shale, and gypsum. This combination is reminiscent of interfingering between lithofacies A and underlying redbeds, although the Timpoweap Member is typically channeled into the Permian Kaibab Limestone and lacks an intermediate Black Dragon equivalent in southwestern Utah.

In summary, a comparison of regional facies supports local data which suggest that the Sinbad Limestone of the Teasdale Dome was basically a shoreline carbonate sequence deposited during a time of farthest advance of the Sinbad seaway.

PALEONTOLOGY

Fossils from the Sinbad Limestone Member represent a relatively restricted molluscan fauna, dominated by pelecypods and gastropods. Preservation is generally poor, owing to the transported and abraded nature of most fossils, as well as subsequent recrystallization and dolomitization. With the exception of minor lag deposits in lithofacies A, all recognizable body fossils came from subtidal rocks in lithofacies B, D, and the lower transition beds of lithofacies E.

Bivalves are ubiquitous in all subtidal facies and are especially numerous in coquinoid skeletal grainstones. Bivalve skeletal material is especially prone to recrystallization, making identification difficult. Two suites seem to be predominant on bedding-plane exposures, and while not mutually exclusive, most slabs are remarkably monogeneric (plate 1, figs. 8, 9). The *Aviculopectin* suite contains both mature and immature *Aviculopectin* sp. and similar small pectinoids and is most common throughout lithofacies B and D, where it appears to compose entire bioclastic units up to 15 cm thick. The *Myalina-Pleuromya* suite is concentrated in the oolitic rocks of the lithofacies D-E boundary, where small (<2 cm), disarticulated valves are usually the only fossils present. Although both suites are probably death assemblages, the byssate *Myalina,* and the free-swimming *Aviculopectin* are both indicative of near normal marine salinities. Other bivalves recovered include several poorly preserved specimens of *Pleurophorus* sp., *Bakevellia* sp., an elongate form similar to the Permian genus *Aviculopinna* sp., and numerous unidentifiable clamlike forms which represent at least two additional genera.

Gastropod occurrence generally parallels that of the pelecypods with the exception of several well-sorted gastropod coquinas in lithofacies A. Whole gastropods are preserved exclusively as steinkerns and include both high-spired and low-trochospiral forms. Identification, even to genus, is questionable, but *Murchisonia* sp. and *Worthenia* sp. are possibly two of the several forms represented.

Ammonoid occurrence in the Sinbad Member is restricted to middle beds of lithofacies D, except for one questionable occurrence in the lithofacies B rocks of the Capitol Wash section. Two-thirds of the several dozen specimens collected came from one especially productive horizon less than 50 cm thick in the Torrey section.

Collections are dominated by *Meekoceras* sp., probably *M. gracilitatis,* followed by *Wyomingites* sp. Part of a coarsely ribbed conch similar to *Wasatchites* sp. was also recovered (plate 1, figs. 1–5). *Meekoceras* sp. and *Wyomingites* sp. are characteristic of the *Meekoceras* zone (Kummel 1954), whereas *Wasatchites* sp. is typical of the younger *Anasibirites* zone. Both zones are assigned an Early Triassic (Scythian) age.

A hexactinellid sponge was the most remarkable paleontological discovery made during the study. Two specimens, poorly preserved as limonite stains, were recovered in the Torrey section from the peloidal mudstone-wackestone subfacies of lithofacies D. Both specimens are frilled, tubular sponges about 12 cm long with an unfused lyssakid skeletal net composed of at least two sizes of spicules, arranged in an overlapping diagonal pattern (plate 2, figs. 2, 5). This is the first report of a sponge from the Sinbad Limestone although sponges have been documented from the Thaynes Limestone (Rigby 1967) in the Wasatch Range.

Miscellaneous fossil material included echinoid plates and spines, crinoid columnals, assorted algal debris, a possible scaphopod, and several ostracodes. One specimen of a lingulid inarticulate brachiopod was also recovered. Although the exact stratigraphic position of the brachiopod in the Sinbad section is not known, lingulids generally represent deposition in shallow water (Tasch 1973, p. 294), under conditions of variable salinity.

Ichnology

Trace fossils are locally abundant in the Sinbad Limestone Member, but the limited number of forms present suggests that the responsible organisms were relatively restricted. Vertical burrows of *Skolithos* and U-shaped burrows lacking a spreite, such as *Arenocolites,* are the most common and wide-ranging trace fossils in the member. *Skolithos* is the only form present in lithofacies A and was found intermittently in all subfacies, including the stromatolitic boundstone. Pascichnid grazing traces and horizontal tubes were observed in the cyclically bioturbated beds of lithofacies B, but do not comprise a significant portion of the ichnofauna until the occurrence of *Planolites* and traces of larger bedding-plane filter feeders in the channel bottoms of lithofacies C.

Trace fossils in lithofacies C and E are most abundant on rippled surfaces, in areas of at least partial subaqueous exposure. Sellwood (1978, p. 264) described from Andros Island similar reworking in tidal channels by organisms probably seeking relief from the intermittent drying. Modern trace fossils from littoral and sublittoral carbonates are described by Kennedy (1975, p. 388) as being typical of the *Cruziana* ichofacies, in which horizontal traces dominate over vertical. Beds from the Sinbad Member that would be included in the *Cruziana* ichnofacies are only limited horizons from lithofacies B and channel bottoms of lithofacies C. Most of the trace fossils in the member fall into the *Skolithos* ichnofacies, which is interpreted by Seilacher (1967) to represent shallow-water, intertidal deposition.

DIAGENESIS

Diagenetic fabrics are the rule rather than the exception in most lithofacies of the Sinbad Limestone Member. Neomorphic recrystallization of matrix and allochems is common in lithofacies B and D, and several forms of dolomitization dominate lithofacies A, C, and E. Claystones of lithofacies F show minor formation of dolomicrite but are generally the least altered rocks in the Sinbad. Late mobilization of calcite to fill voids and leaching (dissolution) of selected grains are additional diagenetic changes that have an important effect on present porosity and permeability.

Recrystallization

Matrix recrystallization is commonplace in limestone and dolomitic limestone of the subtidal lithofacies. The majority of these rocks are packstones and as such originally contained interstitial mud. Evidence for formation of micro- and pseudospar includes (1) gradational contacts between grains and matrix crystals, (2) generally uniform crystal size, (3) patches of unaltered mud, and (4) mud-filled fossils in a sparlike matrix. Recrystallization is also indicated by the presence of initially grain-supported allochems now floating in more matrix spar than would have normally grown between them. Had the interstitial material been original spar, it would have filled only the intergranular voids, but neomorphic growth of pseudospar from micrite could have expanded the matrix producing the floating grains. Folk (1974) reports that microspar and pseudospar seem to form in a diagenetic environment low in magnesium ions while unaltered micrite is the stable product in a magnesium-rich environment. Such an interpretation explains the presence of neomorphic spar in lithofacies B and D, which represent normal salinities, and suggests that the dolomitic lithofacies probably never had extensive recrystallization before dolomitization. This interpretation supports the use of the term *grainstone* rather than *packstone* for questionable rocks of lithofacies E and agrees with the connotation that grainstone carries for higher-energy deposition.

Recrystallization of selective allochems, on the other hand, is common in all facies and seems controlled only by the original composition. Bivalves often show differential recrystallization of inner and outer valve margins due to less stable layers of aragonite. Gastropods are less prone to pervasive recrystallization, and echinoderm fragments are rarely altered. Oolites are commonly recrystallized except in dolomitic packstones. Recrystallized allochems are important because they appear much more prone to leaching and dissolution (fig. 9). When matrix and allochems are both severely altered, uncrystallized micrite envelopes are often the only evidence of original composition.

Dolomitization

The occurrence of dolomite, the dominant rock type in the Sinbad Member of the study area, can be conveniently separated into two groups, the homogeneous dolomites of lithofacies A and C and the heterogeneous dolomites of lithofacies E. The presence of dolomite in subtidal rocks is less common but is most similar to that of lithofacies E.

Homogeneous Dolomite

Rocks of lithofacies A and C are interpreted in other sections of this report to represent deposition in the supratidal and intertidal zones of a carbonate shoreline environment. Dolomitization in modern carbonate tidal flats has been widely documented in studies by Shinn and others (1965, 1969) from the Bahamas, and Illing and others (1965), and Hsu and Schneider (1973) from various portions of the Persian Gulf. The main process involves the replacement of primary calcite and especially aragonite by reaction with Mg-rich groundwaters that accumulate in areas restricted from normal marine influx, and subjected to sufficient evaporation to initiate the precipitation of gypsum or anhydrite. When the Mg/Ca ratio approaches 10 (Asquith 1979, p. 21), replacement begins. This type of syngenetic (used here as penecontemporaneous) dolomite is characteristic of the supratidal-sabka zone where it produces dolomitic crusts up to a foot thick (Lucia 1972, p. 163).

Dolomites from lithofacies A and C meet the following criteria of Chilinger and others (1979, p. 464) and Asquith (1979, p. 22) for syngenetic dolomitization: The individual grain size is very fine, generally less than 10 μ. The fabric ranges from xenotopic to idiotopic with the matrix uniformly replaced. Associated rocks include evaporites, and are generally peritidal in origin (peritidal origin for lithofacies A was established independent of dolomitization). Rocks display a restricted fauna, indicative of hypersalinity. Sedimentary structures include stromatolitic bedding and evidence of subaerial desiccation.

Dolomitization within lithofacies A and C is generally uniform from section to section, except for an increase in calcite in the packstone subfacies toward the northwest. Open marine conditions prevailed to the northwest (fig. 6), eventually grading into normal marine environments that produced the Thaynes Limestone, so such a northwestward decrease in dolomite is consistent with syngenetic dolomitization, basically a shoreline process.

The hypersaline interstitial waters responsible for syngenetic dolomitization are envisioned to move in several different ways. Although it is not within the scope of this report to compare methods of dolomitization, the four primary models are mentioned for later reference to contrasting dolomitization of lithofacies E.

1. The capillary fringe model (Hsu and Schneider 1973) suggests vadose water ascends by capillary action during evaporation.
2. The seepage reflux model (Deffeyes and others 1965) postulates downward descending hypersaline brines (e.g., from a supersaturated lagoon).
3. The evaporative pumping of seawater model (Hsu and Schneider 1973) postulates ascending Mg^{2+} concentrated seawater.
4. The evaporative pumping of groundwater model (Hsu and Schneider 1973) suggests ascending Mg^{2+} concentrated groundwater.

Although the seepage reflux model seemed to be the favorite of most workers, Hsu and Schneider (1973, p. 421), as a result of their work on the Abu Dhabi sabka, maintain that the evaporative pumping of groundwater model is probably the closest to reality.

Heterogeneous Dolomites

Dolomites of lithofacies E are referred to as heterogeneous to distinguish them from the fine-grained, uniform dolomite of lithofacies A and C. These upper dolomite beds involve differential dolomitization of allochems and matrix and a dramatic upsection increase in the magnitude of dolomitization from bed to bed. Crystal size is extremely variable, ranging from dolomicrite to very coarse (0.3-mm) euhedral dolorhombs that are typically zoned (fig. 27). An intriguing contrast between lower and upper beds of the lithofacies is the change from coarsest rhombs occurring in allochems in the lower beds to having coarsest rhombs restricted to matrix in upper beds (figs. 29 and 30). In general, were it not for other evidence showing that the dolomitization is shoreline controlled, the variability and coarseness of the dolomite is more indicative of a later diagenetic, rather than syngenetic, origin.

Rocks from lithofacies E are mainly well-sorted grainstones which are interpreted to represent near-shore bars or shoals. These shoals show evidence of tidal reworking and channeling and at least partial subaerial exposure. Dolomitization in these rocks is obviously different from the syngenetic peritidal do-

lomitization interpreted for lithofacies A and C. A regressive return to shoreline sedimentation is indicated following the offshore deposition of lithofacies D, but gone are the evaporites and algal mats which characterize an upper tidal flat origin. The sorting, geometry, and sedimentary structures are also indicative of accumulation in a higher-energy environment.

A possible solution is offered by Chilinger and others (1979, p. 464–65), who reported similar dolomites from the Little Falls and Lockport Formations, which satisfy criteria for deposition in a syngenetic environment but whose dolomitization clearly occurred later than what is usually considered penecontemporaneous. The somewhat cumbersome term *postpenecontemporaneous* is applied by Chilinger and others (1979) for these dolomites which are neither purely syngenetic nor late diagenetic. They postulate dolomitization from a sea-meteoric water mixture, drawing upon the large supply of Mg ions rather than a large Mg/Ca ratio, and cite examples of considerable variation in crystal size like that found in lithofacies E.

Another possibility, more to my liking, is proposed by Jacka and Franco (1975) to explain a "diagenetic" type dolomitization in intertidal and subtidal facies rocks. In this hydrodynamic dolomitization model (really a special case of the previously described evaporative pumping of groundwater model), the diagenetic dolomite results from an influx of Mg-rich meteoric groundwater at shallow depth shortly after burial. The groundwater moving through the supratidal zone becomes charged with magnesium, and a phase of microcrystalline dolomitization results as the waters move into the intertidal and upper subtidal zone. As the waters move farther into the subtidal zone, nucleation becomes more isolated because of lower Mg-concentration, and coarser crystalline sucrosic dolomite is formed. As shoreline geometry and hydrostatic pressure fluctuate, different phases of micro- and macrocrystalline dolomite could be found together, as in the Sinbad Member.

The feasibility of the preceding models is partially dependent on the paleocoastline, depth of burial, and permeabilities of unlithified sediments. The dolomitizing fluids of Jacka and Franco (1975) crossing from the sabka to the oolite-peloid shoals may be impeded by lagoonal muds. Lagoonal conditions, believed to be present during deposition of lithofacies B, could have disappeared or, as in the Persian Gulf, prograding shoals may actually impinge on the coast without an intervening subtidal zone. The hydrodynamic dolomitization model, despite its problems, seems to explain better the variable crystal size as a function of differential nucleation due to waning Mg-concentrations.

On the other hand, models based on sea-meteoric water mixtures (Land 1973, Hanshaw and others 1971) could explain differential dolomitization simply by individual variation in allochem chemistry, rendering them less subject to the coarse dolomitization found in the matrix, or by multiple phases of fluid movement of varying concentrations as suggested by iron zoned dolorhombs that form during periods of uniformly fluctuating conditions (Scholle 1978). Both of the above explanations, however, could also be applied to explain variations in the hydrodynamic model.

The fact that dolomitization increases upsection as regressive conditions prevail suggests hypersaline meteoric water rather than seawater was the dominant medium for dolomitization and further supports the model of Jacka and Franco (1978).

In summary, all dolomitization in the Sinbad Member is early, in the sense that it predated deep burial or lithification. Dolomites of lithofacies A and C are confidently assigned a syngenetic time frame, and those of lithofacies E are probably both syngenetic and postpenecontemporaneous. Detrital dolomites, those which result from reworking of disaggregated rhombs from previously lithified dolomitic crusts, are well documented in subtidal rocks (Chilinger and others 1979, p. 485) and were suggested by Blakey (1974, p. 32) to possibly explain the occurrence of some dolomitic fabrics in the Sinbad beds. The writer agrees that the rare, large dolorhombs in some limestone units could be blown or washed in from sabka flats, but their presence is negligible and does not constitute an important percentage of the Sinbad dolomites, which generally indicate an in situ replacement origin.

DEPOSITIONAL ENVIRONMENTS OF CARBONATE LITHOFACIES

Lithofacies A

Stromatolitic Boundstone Subfacies

Following Black's (1933) discovery of modern stromatolites on Andros Island, study by industrial and academic researchers has yielded voluminous literature on algal stromatolites. Although both subtidal and deep-water (Playford and Cockbain 1969) stromatolites have been described, the great majority of recent examples and fossil counterparts are related to tidal-dominated, shallow, carbonate shorelines. In fact, algal stromatolites are considered by many to be the most diagnostic organic feature of tidal-flat sediments (Lucia 1972, p. 162).

Stromatolites have been divided into numerous types, both generic and geometric, but the fundamental dynamic process which characterizes them and the resulting boundstones is simple. Colonies of coccoid and filamentous blue-green algae, in mounds and rubbery mats, trap sediment washed over them by tides or storms on their sticky, mucilaginous surfaces. As successive layers of sediment are added, the algal mat thickens, and new algae grow on the upper surface. Laboratory experiments demonstrate that algal mats buried by millimeters of sediment can reform their upper surface in less than 24 hours (Ginsburg and others 1972, p. 12.1).

Active algal mats are spatially confined by the limits of alternate wetting and drying, and where present, by algal-grazing cerithid gastropods (Sellwood 1978, p. 265). Thus they are primarily found in the high intertidal or low supratidal environment (Lucia 1972, p. 162). Tidal channels, where scouring effects are concentrated, and splash pools that are usually underwater are not conducive to continuous growth of the mats (Sarjeant 1975, p. 175).

The stromatolitic boundstones of the Sinbad Limestone are similar to most fossil algal mats in that the original algal filaments are not preserved, but have a characteristic fenestral fabric of trapped intraclasts which were washed over the algal surface. Thick storm-surge accumulations, which are common in many ancient and recent stromatolite deposits (Bathurst 1978; James 1979), are apparently less important in the Sinbad beds. Absence of storm deposits is probably due to dampening of wave energy by the broad, shallow Moenkopi shelf (Blakey 1974), over which all but the most severe storm and wave energy would have been dissipated long before reaching shore. Geopetal filling of some fenestrae by mud (now dolomicrite) and discontinuous dolomicrite lenses are evidence of adjacent fine-grained sediment washing onto the binding surface of the algal mats.

Desiccation features, such as curled dolomicrite chips and prism and sheet creeks found in the subfacies, are to be expected in the algal mat environment which is characterized by alternate subaerial-subaqueous exposure. Birdseye and laminoid fenestrae found in the subfacies are typical of modern algal-mat and tidal-levee areas and result from desiccation (Wilson 1975, p. 82), gas heave from decay of organic matter (Sellwood 1978, p. 265), or both (James 1979, p. 112). The tepee structures common in some units bear a remarkable resemblance to modern tepees of the Sabka Matti area of the Trucial Coast (Evamy 1973, p. 334) and ancient counterparts from the Permian of west Texas (Newell and others 1953, p. 128). These structures are caused by desiccation joints which undergo subsequent internal calichefication (Smith 1974), arching the laminae upward, tepee-style. Such prolonged drying and crystallization require maximum exposure and seem to be indicative of the supratidal zone. The high intertidal-supratidal interface is also suggested by the LLH (Logan and others 1964) geometry of the stromatolites and relative paucity of whole fossils.

Oolite-peloid Packstone Subfacies

The intertidal zone of modern carbonate shorelines is characterized by a complex system of tidal channels (fig. 32). Shinn and others (1969, p. 1202) have compared the environment to a "river turned wrongside out," with the tidal channels providing sediment from the marine substrate to the littoral zone.

Peloids, pellets, and abraded bioclasts of the lithofacies A packstones probably had their origin in subtidal lagoons and were subsequently transported onto the tidal flat or accumulated as bars in tidal channels during normal diurnal tides and storms. The process parallels that of the stromatolitic boundstone, except the transported material is not trapped and assimilated in algal mats. Poorly sorted lime sand, similar to this subfacies of the Sinbad Member, is commonly reported from the intertidal zone of the Bahamas (Shinn and others 1969, p. 1207) and Persian Gulf (Wagner and Van Der Togt 1973, p. 137–41).

Although found together in the Sinbad rocks, pellets, peloids, and skeletal material usually accumulate in the more hospitable subtidal zone while oolites indicate a somewhat higher-energy environment. Their presence in the same rock is typical of modern sedimentation patterns from the Persian Gulf where Purser and Evans (1973, p. 279) report bars of rippled oolites at the mouths of tidal channels emptying into areas of lagoonal deposition. These oolites have been observed forming within the tidal channel and even in some parts of the lagoon.

Energy variation in and adjacent to these channels is rapid, explaining the cross-bedding and ripple marks of the subfacies while still allowing for the muddy matrix. Tidal channels behave similarly to unidirectional rivers and show evidence of migration, scour and fill, and point-bar formation, all of which were observed from this subfacies. Channel transportation from

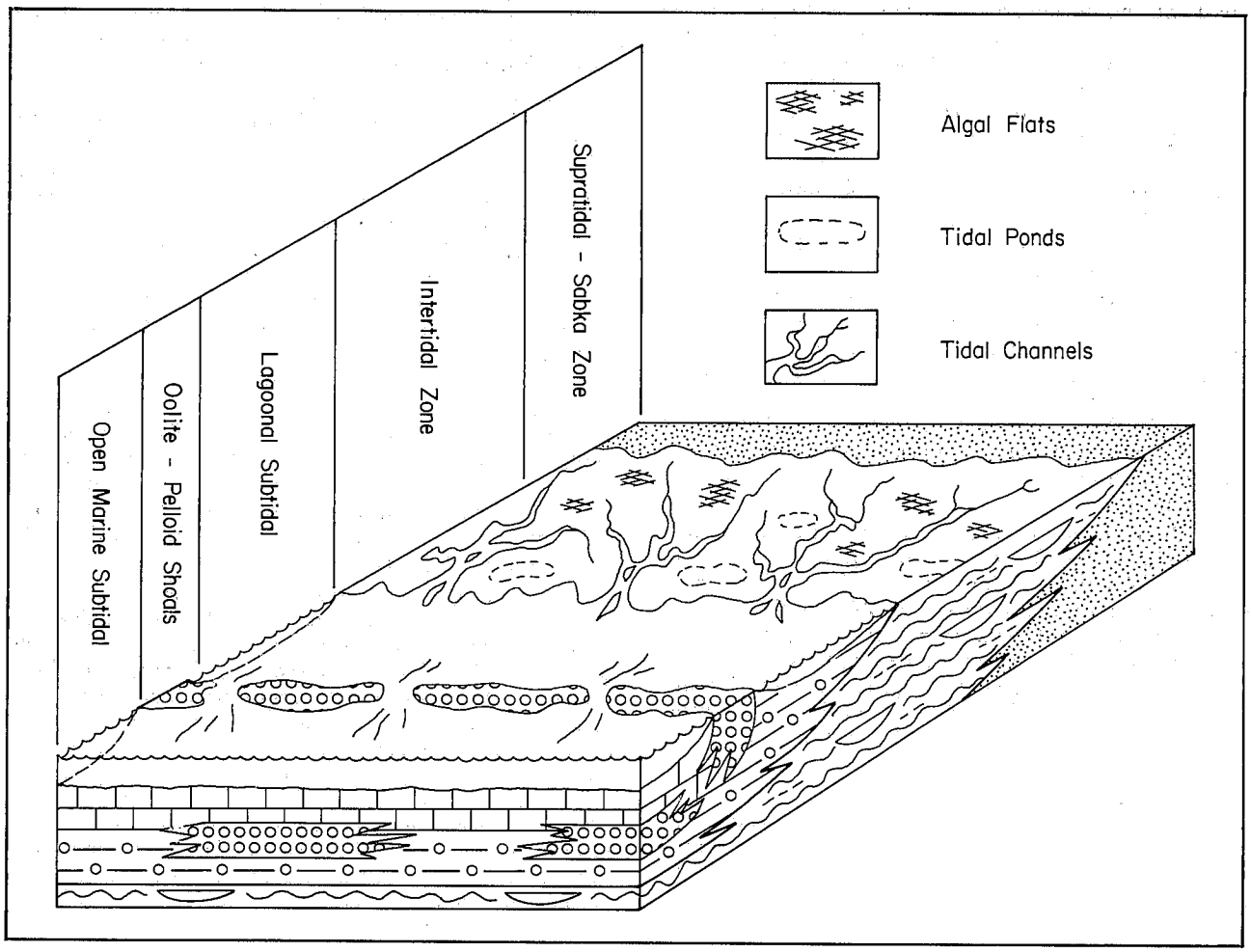

FIGURE 32.—Diagram showing relationships of depositional environments along the Sinbad shoreline.

the subtidal zone also accounts for the presence of echinoderm fragments in rocks which otherwise represent hypersalinity. The oolite-peloid packstone subfacies probably accumulated in channel bars rather than on the bottom of the channels if we are to judge from the less intense bioturbation found in the unstable, shifting sediments of the bars, as opposed to the heavily populated channel bottoms.

Dolomicrite Subfacies

Several related but separate environments are indicated by rocks of the dolomicrite subfacies. Low areas between channels within the intertidal zone of modern carbonate shorelines are commonly filled with tidal ponds (fig. 32). Sediments accumulating in these ponds are typically fine-grained muds with remnant peloidal structure (Sellwood 1978, p. 268). Interchannel pond sediments are usually featureless. Shinn and others (1969, p. 1208) attributed this lack of features to homogenization by bioturbation, but it may under proper conditions show lamination. Massive dolomicrites from the Sinbad Member were probably deposited in similar tidal ponds, on the basis of lithology and position with respect to stromatolitic boundstones, since ponds are commonly fringed by algal mats.

Rippled dolomicrites showing micro-cross-laminae and carbonate flaser bedding require deposition under slightly more agitated, but still shallow, conditions. Although masked by dolomitization, these rocks represent originally pelletal-peloidal intraclasts which were reworked by tidal activity in areas spared from intense bioturbation. James (1979, p. 113) reported rippled and scoured dolomites from well-drained supratidal zones which are often covered by a thin film of algal mat. Flaser bedding in clastic tidal flats is common in tidal channels. Reineck and Singh (1975, p. 359) and Shinn and others (1969, p. 1207) reported some channel bars in the Bahama Islands can contain considerable amounts of soft pelletal muds. Rippled dolomicrite probably formed on the upper tidal flat where channel-bar sediments are finer grained, and hypersalinity limited the organisms responsible for extensive bioturbation.

Cryptalgal dolomicrites, without fenestrae but with wavy irregular bedding, are commonly described from the supratidal zone of modern and ancient carbonate flats (Lucia 1972, p. 188; Braun and Friedman 1969, p. 113). Such dolomicrites are probably similar to the stromatolitic boundstones, but because of the rare inundation of the supratidal zone the resulting algal films are thin and infrequent. The limited organic material available for decomposition probably explains the absence of gas-heave vugs found in the more luxurious algal mats.

Channel Conglomerate Subfacies

As previously described, intertidal zones are dominated by channel complexes which are the main pathways for tidal current exchange. Depth of channels may vary from several centimeters to several meters, with channel junctions in the Persian Gulf up to 13 m deep (Bathurst 1978, p. 195). Shinn and others (1969, p. 1206) noted that sediment from tidal channels showed the greatest variability in size of the entire tidal flat.

The channel conglomerate subfacies in the Sinbad Member is characterized by discontinuous lenses of intrafacies-derived lithoclasts of pebble and occasional cobble size which represent bedload deposition under the highest-energy conditions observed in the member.

Sellwood (1978, p. 268) noted that normal migration of tidal channels can incorporate larger clasts derived from undercut levees, but the rarity of channel conglomerate rocks in the Sinbad beds suggests periods of intense but infrequent energy. Storm surges of high tides and waves rolling across the flats could rip up pieces of desiccated algal mats and dolomitic crust and funnel them back through the tidal channel. The lack of uniform imbrication of flat pebbles, which precluded current determination, is probably a result of the bimodal reworking by incoming and outgoing tides. Similar conglomerates from the Tribes Hill Formation (Lower Ordovician) of New York were interpreted as being channel derived by Braun and Friedman (1978, p. 113).

Evaporite Subfacies

The presence or absence of primary evaporites in the carbonate shoreline environment is basically a function of climate. The classic study areas of modern deposition, the Bahamas and the Persian Gulf, differ mainly in their respective amounts of dolomite and gypsum, which can be directly related to the humid climate of the former and arid climate of the latter. Intense evaporation in an arid climate concentrates surface brines and initiates upward capillary movement from the water table (Bathurst 1978, p. 525). The resulting high salinity encourages the precipitation of gypsum-anhydrite, which in turn raises the Mg=Ca ratio, causing subsurface dolomitization. Although deep-water evaporite models are known (Schmalz 1969), the interrelation of the gypsum-dolomite process makes environmental interpretion of rocks in which they mutually occur quite exact. Authigenic growth of primary gypsum in dolomitic sediments is essentially a supratidal phenomenon.

Gypsum occurs in the subfacies in bands of discrete nodules, similar to modern deposits from the Persian Gulf (Schneider 1975, p. 213; Kinsman 1969, p. 836). The gypsum is precipitated in situ from hypersaline pore water within the dolomicrite, as evidenced by its displacive growth, but, because of its high solubility, gypsum is often removed during diagenesis. Possibly much of the original gypsum from the subfacies was removed by leaching, although collapse features which document such dissolution (James 1979, p. 116) were not observed.

Beds of massive, ptygmatic gypsum, such as those discovered in the South Draw section, represent continued growth and coalescence of individual gypsum nodules (Kendall 1979, p. 152). Such growth often leaves host sediments, in this case dolomicrite, as disrupted partings (fig. 16). The increase of gypsum to the southeast parallels the trend of pervasive dolomitization.

Lithofacies B

The subtidal environment is an important and diagnostic component of all carbonate shorelines. In modern deposits and ancient analogs, two main subdivisions are recognized: the open marine shelf and the protected lagoon (fig. 32). James (1979, p. 110) noted that lagoonal geometries in modern examples are extremely variable, ranging from a broad, expansive lagoon in the Bahamas, to narrow elongate types in the Persian Gulf, to small pocket bays of Western Australia. Sediment accumulating in lagoons consists of pelletal muds and silt-size carbonate grains with varying amounts of skeletal material (Shinn 1973, p. 181). Primary sedimentation structures are usually lacking owing to the extensive bioturbation which characterizes lagoonal deposition.

The skeletal packstone and pelletal wackestone subfacies of lithofacies B are interpreted to represent deposition in lagoons which lay shoreward of the tidal flats of lithofacies A (fig. 32). Normal sedimentation in the lagoon consisted of pellets and peloids, many probably of algal origin (H. J. Bissell personal communication 1980), with variable influx of oolites from tidal

channels or shoreface shoals and transported skeletal debris. Codiacean algal fragments, observed in several thin sections, are commonly assigned to a lagoonal environment (Ginsburg and others 1972, p. 10.2). The general decrease in faunal diversity (with respect to lithofacies D) may represent salinity increases common in restricted lagoons. Progressive increases in salinity from the outer platform to the shelf lagoon of the Bahamas have been reported by several authors (Newell and others 1959, fig. 5; Purdy 1963, p. 338). Modern lagoonal sediments accumulating in the Persian Gulf (Evans and others, p. 261) are similar to those of both subfacies but seem to contain more mud and fewer skeletal allochems, with wackestones favored over packstones.

The influx of skeletal material and the cyclic nature of the bioturbation in the Sinbad beds are related in the following way. High spring tides or storm surges bring large quantities of fragmented skeletal debris into the lower-energy lagoon. Most of the bioclasts have their origin on the faunal-rich shelf and are broken at the surf zone of the protective shoal, and are then brought in through the numerous tidal channels. After a return to quiescence, the resultant grainstones are subsequently overlain by normal pelletal sediments which become thicker and increasingly bioturbated until the cycle is repeated by the surge of another storm. The churning effects of continuous bioturbation and normal compaction would mix the abraded bioclasts with pellets, peloids, and oolites, resulting in the present fabric of grain-supported packstone with remnant layers of grainstone.

The pelletal wackestone subfacies represents deposition under similar but different conditions, and any interpretation must take into account the significant decrease in skeletal material, increase in pellets, increased dolomitization, and presence of planar cross-bedding. These changes certainly represent a shoreward shift in sedimentation, but the limited extent of the wackestone interbeds precludes a major regression, as in lithofacies C, and suggests local, probably paleocoastline, variations. Purser and Evans (1973, p. 226) described a possible analog from the Persian Gulf in which indurated pellets are occasionally reworked into bars at the convergence of tidal channels and lagoons. Such an environment of locally increased agitation could explain the selective sorting and cross-bedding found in the subfacies, while the partial subaerial exposure of the bars would be less conducive to fossils and more prone to dolomitization. The migration of bars into the adjacent lagoon would also agree with the interfingering observed between the two subfacies.

Lithofacies C

The depositional reconstruction of lithofacies C is both complicated and perhaps simplified by the homogeneous dolomitization that characterizes the sequence. Although original fabrics have been largely destroyed, the channeling and the peritidal nature of the dolomitization suggest a return to tidal-flat conditions. Stratigraphically sandwiched between rocks of subtidal origin, the unfossiliferous dolomites of lithofacies C represent a period of temporary but widespread regression of the Sinbad shoreline. Such rapid fluctuation seems common in the Early Triassic and has been recognized in the Virgin Member of the Moenkopi Formation (Belnap 1971, p. 147) in the Thaynes Limestone (Newman 1974, p. 74).

Withdrawal of the lagoonal waters of lithofacies B exposed the pelletal muds to reworking by tidal channels, and the ensuing hypersalinity contributed to dolomitization. Paucity of fossils and bioclasts, in general, in all sections of the lithofacies is probably due more to hostile salinities than destruction by diagenesis. Locally extensive bioturbation, common in rippled channel bottoms of lithofacies C, is diagnostic of muddy channel sediments in modern intertidal zones that are regularly filled with water from normal tidal exchange (Shinn and others 1969).

The channel size in lithofacies C is much smaller than similar channels from lithofacies A, and bedload conglomerates are lacking. These lower-energy conditions may be related to the observation that the tidal flat of lithofacies A was transgressive while that of lithofacies C was regressive. Shinn and others (1969, p. 1226) observed that channels on regressive tidal flats are usually less extensive and less numerous than those developing on transgressive shorelines.

Lithofacies D

Limestone of lithofacies D documents the abrupt return of marine conditions to the study area. While some of the renewed subtidal sedimentation was similar to the lagoonal packstones and wackestones of lithofacies B, evidence suggests most deposition took place under less retricted, more nearly open marine conditions.

The oolite-mollusk packstone subfacies was partially deposited on the seaward, rather than the lagoonal, side of oolite shoals. Pellets gave way to oolites, and echinoderm fragments increased at the expense of codiacean algal debris. Occasional burrows replaced total bioturbation, and articulated bivalves are increasingly common. The seaward shift in deposition is also indicated by an occasional ammonoid conch.

The peloidal mudstone-wackestone subfacies represents the lowest-energy, most basinward deposition in the study area. The position of the subfacies between underlying and overlying beds of oolite-mollusk packstone marks the maximum transgression of the Sinbad seaway. As a parallel, in the deeper water along the axis of the Persian Gulf, modern carbonate mud with minor skeletal and terrigenous material is accumulating (Heckel 1972), under conditions probably similar to those of this subfacies of lithofacies D.

Normal marine salinities are indicated by a moderately diverse suite of ceratite ammonoids. Conches of these ammonoids were found in a variety of orientations, many supported at high angles to bedding (plate 1, fig. 5), as if they settled into an oozy, muddy substrate. Normal salinities and deposition well below wave base are also indicated by the preservation of sponges. Lyssakid sponges, like those found in this lithofacies, contain unfused skeletal elements which are held together only during the life of the sponge. Preservation of the relatively intact spicule net suggests rapid deposition and burial on a substrate of minimal turbulence.

Lithofacies E

Barrier bars or shoals are common along carbonate shorelines, where coated grains and indurated pellets are subjected to reworking by shoreface processes of moderate to high energy. The lagoonal environment owes its existence to these protective shoals which serve to buffer the energy of waves, tides, and currents. Conversely, the agitated water and abundant fragmented material for nuclei create an environment well suited to the formation and accumulation of the coated grains which often make up the shoals and bars.

The well-sorted, cross-stratified grainstones of lithofacies E were deposited on similar shoals which probably formed at the high-energy interface between the lagoon and open marine shelf (fig. 32). These grainstones were deposited in the final regressive phase of the Sinbad Limestone and formed shoals

which followed the receding shoreline back to the north and west.

Tidal channels commonly breached the shoals of lithofacies E, as evidenced by lenses of herringbone cross-bedding and the presence of large channels oriented normal to the strike of the shoals. Work in the Persian Gulf suggests bidirectional tidal currents through the bars are an excellent oolite-producing environment because of the constant alternation between low and high energy (Loreau and Purser 1973, p. 280). Many of the shoal-making allochems in the Sinbad Member, however, are peloids and not coated grains. The presence of both is consistent with modern deposition in the Umm al Quajwain region of the Trucial Coast where coalescence of tidal deltas has formed barrier complexes 15 km long, composed entirely of sand-sized pellets (peloids of this paper) (Purser and Evans 1973, p. 227).

The upward decrease in bioclasts throughout lithofacies E is more than the result of selective sorting and suggests original scarcity. Sellwood (1978, p. 269) notes that mobile belts of carbonate sand often have an impoverished benthonic fauna due to the high instability of the substrate.

Lithofacies E in the southeast sections appears to interfinger with the underlying limestones of lithofacies D. This part of the study area approaches the farthest southeastern advance of limestone deposition, and interfingering of the shoal and shelf facies probably records several migrations of the shoal seaward. Purdy (1961, p. 60) noted that oolite shoals on the Bahama Platform prograded in the direction of maximum tidal flow when the rate of sea level rise was exceeded by the rate of oolite accumulation. If interfingering in the Sinbad rocks occurred at maximum stillstand of the shoreline, as it apparently did, with favorable oolite production, shoal progradation would parallel ebb tide direction and migrate seaward.

Dolomicrite layers in lithofacies E, many of which are found in southern sections as flat-pebble conglomerates, were probably washed over the shoals as mud stirred up by high tides or storms. Some of the dolomicrite layers have desiccation cracks on ripple marks, attesting to at least limited subaerial exposure of the shoals. Flat-pebble conglomerates in southern sections are probably not current transported but are formed in situ by expansive desiccation of dolomicrite into polygons that were subsequently weathered in place. Similar in situ flat-pebble conglomerates were described from the Lower Ordovician of New York by Braun and Friedman (1978, p. 85). Larger desiccation polygons and edgewise conglomerate are not common on shoals and suggest parts of lithofacies E in the southern sections may grade into the tidal flat, representing conditions similar to those of lithofacies A.

Lithofacies F

The dolomitic claystones of lithofacies F signal the beginning of the end for carbonate sedimentation in the Sinbad seaway. In the Teasdale Dome the complete regressive cycle of subtidal through supratidal progressed only as far as the shoal grainstones of lithofacies E before clastic deposition abruptly returned to the area. In sections regionally to the south and north, Blakey (1974, 1977) reports a complete supratidal sequence for facies equivalent to lithofacies E, including stromatolitic boundstones and sandy supratidal dolomites.

Claystones of lithofacies F represent the fine-grained prodelta sediments which heralded the advance of the overlying Torrey delta. The influx of terrigenous material first mixed with the Sinbad carbonates but quickly took over altogether and inhibited further growth of calcite- and aragonite-producing fauna and flora.

Minor skeletal debris, peloids, and dolomitic cement attest to the marine origin of the claystones which rapidly become more terrestial-appearing upsection. Tidal action played an important role until the end, however, as evidenced by lenses of herringbone cross-bedded peloidal packstone. These lenses occur less and less frequently upsection, finally giving way to homogeneous claystone.

DEPOSITIONAL SUMMARY

The Sinbad Limestone Member in the Teasdale Dome is characterized by three depositional phases (fig. 33): the transgressing tidal flat–sabka of lithofacies A, the subtidal sedimen-

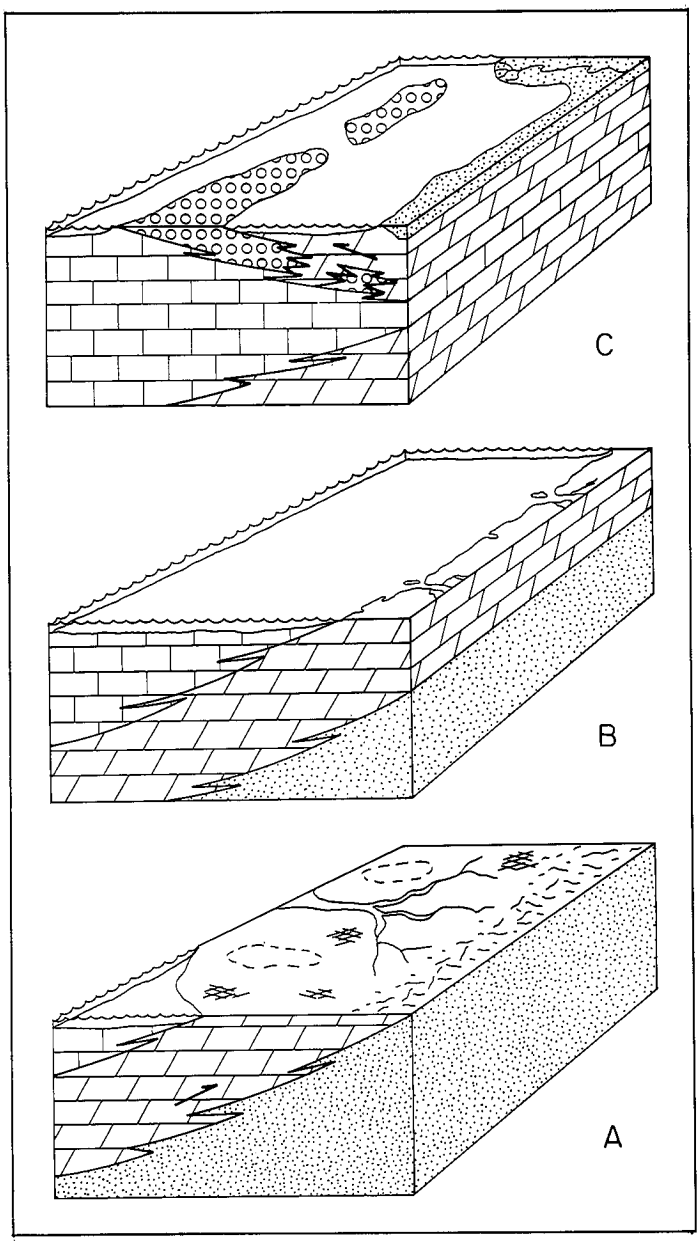

FIGURE 33.–A.–Transgressing tidal flat-sabka of the first phase of deposition of the Sinbad Member. B.–Subtidal deposition of the second phase during the period of maximum advance of the Sinbad seaway over the study area. C.–Final phase of deposition characterized by formation of grainstone shoals during regression of the Sinbad shoreline. Clastic sediments of the incipient Torrey delta eventually end carbonate deposition.

tation of lithofacies B and D, and the shoaling upward sequence of lithofacies E.

Supratidal and intertidal rocks of the first phase mark the impending advance of the Sinbad–Timpoweap sea, which resulted in the most extensive blanket of carbonates in Moenkopi time. Stewart and others (1972, p. 77) estimated that the depositional slope across the broad Moenkopi Shelf was extremely low, approximately 1 foot per mile, and a slight rise in sea level or minor regional downwarping could easily trigger a widespread transgression. Blakey (1974) questioned a tectonically controlled shift and suggested that the underlying Black Dragon redbeds already represented clastic tidal-flat deposition, and the Sinbad carbonates simply represent a substitution of carbonate sediment for the waning terrigenous sediment, without any change in geography or bathymetry. The lower contact of the Sinbad Member is gradational in the study area, in contrast to the deeply channeled contact of the Timpoweap Member (McKee 1954, p. 13), which is also suggestive of a gradual, low-energy transition between siliciclastic and carbonate deposition. Assuming such a decrease in clastic influx, favorable conditions for the rapid shift to precipitation of calcium carbonate include the warm shallow water, an organic-rich platform to the west, and an arid to semiarid climate. Most paleogeographic reconstructions place the Triassic equator only a few degrees south of the present study area (Dietz and Holden 1970, p. 34).

The transgressing carbonate tidal flat of the first phase is shown in fig. 33A. Each component of the flat, represented by a distinct subfacies of lithofacies A, appears separately in the stratigraphic record but when combined becomes diagnostic of the regional environment of deposition. James (1979, p. 111) referring to the interpretation of ancient carbonate tidal flats noted, "The important point to grasp is that numerous environments may exist in very close proximity, not only perpendicular to the shoreline but parallel to it as well, so that in the geologic record rapid, local lithological variations are to be expected, both vertically and laterally." Such is the relationship between subfacies in the first phase of shoreline deposition. Stromatolitic boundstones formed at the high intertidal and supratidal zone. Oolite-peloid packstones were deposited on channel mouths into the adjacent lagoon. Dolomicrites were deposited in intertidal ponds and supratidal flats, while channel conglomerates represent bedload deposition in tidal channels during surges of abnormally high energy, probably storms. Evaporites were restricted to supratidal zones during conditions of general aridity and probably grade into the sabka fringe.

The second main phase of deposition occurred as the subtidal zone advanced over the shoreline (fig. 33B) and deposited carbonates of a lagoonal and open-shelf origin. These are the most calcareous and fossiliferous rocks in the study area and document normal to near-normal marine salinities. Skeletal packstones and pelletal wackestone accumulated in and around the margins of protected lagoons. Peloidal mudstone-wackestone rocks were deposited well below wave base in the deeper-water shelf environment, which lasted only a short time in the study area during the period of maximum transgression.

Deposition during the final regressive phase of the Sinbad Limestone moved landward again with the formation of oolite-peloid shoals which paralleled the receding shoreline (fig. 33C). These well-sorted, cross-bedded grainstones accumulated in the agitated waters of the moderate-energy shoreface environment prior to the termination of carbonate deposition by prodelta fine, terrigenous, clastic sediments of the advancing Torrey delta. The rapid influx of clastic sediment suggests the delta had already prograded outward into the Sinbad seaway adjacent to the study area. Then the main distributary was abandoned, and a new lobe quickly prograded into the Teasdale Dome region depositing terrigenous material and effectively bringing to an end deposition of the Sinbad Limestone Member.

PETROLEUM POTENTIAL

The Sinbad–Timpoweap Member of the Moenkopi Formation has a long history of minor oil and gas production in Utah. The Virgin Field, the state's oldest producing area, was completed in the Timpoweap Member in 1907 at an average depth of 600 feet (Bahr 1963, p. 169). Geologists have long recognized that the member's presence in the breached Laramide upwarps of south central Utah (i.e., San Rafael Swell and Teasdale Dome), with their ubiquitous dead oil saturation, represent exhumed fossil oil fields and document considerable amounts of hydrocarbon migration. Although modest production from the Sinbad Member continues in the Upper Valley field (Garfield County), and shut-in potential exists in the South Last Chance Field (Emery County), recent interest in the member as a potential reservoir has shifted to the hingeline area of central Utah.

The Sinbad Member is much thicker in the Utah hingeline than in the Teasdale study area, and rocks are increasingly more basinal rather than shoreline in origin. The member is faulted down over 3,000 m in some sections and is overlain by a thick sequence of sealing Jurassic evaporites. Recent Phillips-Shell test wells in Sanpete County and along the Wasatch Plateau have yielded excellent subsurface shows (Shell geologists, personal communication 1979) although isolation and environmental concerns have made exploitation thus far economically unfeasible.

In addition to obvious structural plays in the complexly faulted area, the Sinbad carbonates are sandwiched between argillaceous redbeds and have potential for stratigraphic traps as well. Koch (1976, p. 214) visualized numerous possibilities for such traps in subsurface Lower Triassic rocks where westward regional dip coincides with local porosity pinchouts. A possible mechanism for pinchouts exists in the lateral termination of the coarse shoreline dolomites of lithofacies E into the tighter, micritic limestones of the Thaynes Formation.

The source for the abundant dead oil in outcrop and subsurface production and shows is unknown. Spencer (1975) analyzed the regional exploration potential and suggested that oil may be indigenous to the Sinbad Member, a belief shared in part by Bissell (personal communication 1980), who studied similar rocks from the Virgin Member of the Moenkopi Formation in southeastern Nevada (Bissell 1970). The most likely facies for authigenic hydrocarbons in the Sinbad rocks would be the algal- and bioclastic-rich lithofacies B and D, which thicken into the deeper-water platform carbonates of the Thaynes Limestone to the north and west, where oil generation seems favored by deeper burial and a thicker column of rock. Several studies have also pointed to the thick Paleozoic shales and carbonates of western Utah which lie downdip of the Mesozoic rocks as a probable source.

Blakey (1977) doubts the amount of dead oil in outcrop can be attributed to any rock unit within the Moenkopi Formation and also questions the extensive lateral migration required for a Paleozoic source to the west. He favors the thick Carmel–Arapian sequence of Jurassic age as possible source beds, noting that post-Jurassic, pre-Cretaceous tectonic restorations of central Utah juxtapose the Jurassic rocks against the

Moenkopi Formation along the ancient Ephraim fault. Moulton (1976), who proposed the importance of the fault, also believed some parts of the Carmel Formation should be considered as excellent source beds.

Potential of Lithofacies

In the Teasdale Dome, oil impregnation uniformly varies from facies to facies within the Sinbad Member, preferring units of higher porosity and permeability. Saturation is always most extensive in the coquinoid skeletal beds of lithofacies D (and to a lesser extent B) and upper dolomites of lithofacies E. Dolomites from lithofacies A and D are rarely stained, and claystones of lithofacies F show no evidence of hydrocarbon passage at all.

Porosity in the Sinbad Member in outcrop is usually fabric selective and dependent upon secondary diagenetic enhancement or reduction. Dolomitization, at least in the study area, is the single most important source of enhancement on the petrographic level, although Blakey (1977) considered fracturing of greater regional import. Dolomitization generally increases porosity in limestones from 12–13 percent (Murray 1960, p. 73) because of the more compact crystal lattice of dolomite over calcite. This increase appears most evident in the heterogeneous dolomites of lithofacies E, but minor to nonexistent in the dolomicrites and finely crystalline dolomites of lithofacies A and C. Such a differential increase in porosity agrees with Asquith (1979, p. 24), who found from his experience with the major dolomite reservoirs of North America that dolomite of a syngenetic origin is usually too fine-grained to yield significant production. In general, dolomicrites, wherever they appear in the Sinbad beds, are tight and require microfractures for their limited staining. Dolomites of lithofacies C become slightly more stained to the south, where dolorhombs become larger and fabrics more idiotopic.

Boundstones of lithofacies A exhibit spectacular fenestral porosity (point count estimates to 25 percent), where leached of spar and geopetal mud, but voids are rarely interconnected, and the matrix between trapped allochems is generally dolomicritic. Packstones and wackestones of the other subfacies lack intergranular porosities for the same reason. Overall, rocks of lithofacies A show what would have been good primary porosity is now reduced through diagenesis, and they do not contribute to the reservoir potential of the Sinbad Member. Both lithofacies A and C are shoreline facies and probably reach their maximum thickness in or near the study area (fig. 3). As the subtidal facies increase to the northwest, they do so at the expense of the shoreline rocks, which do not constitute a major portion of the member in the hingeline area.

Subtidal lithofacies B and D are little affected by dolomitization and exhibit a variety of porosity types. Fabric-selective porosities such as fossil moldic, oomoldic, and shelter are especially common (fig. 19) but vary considerably from sample to sample owing to the sporadic nature of recrystallization and solution leaching. Blakey (1977, p. 79) suggested such porosities are concentrated along fractures and joints in outcrop, but data from this study failed to corroborate his hypothesis, finding that similar diagenetic fabrics were controlled by depositional units rather than later fracturing. Storm-surge grainstones yielded point count porosities of up to 15 percent and were usually filled with crystalline or tarry asphalt. Rocks of the peloidal mudstone-wackestone subfacies, on the other hand, were unstained because of their lack of stylolites and microfractures and the paucity of allochems to be recrystallized and leached. Subtidal rocks thicken to the northwest and comprise the majority of the Sinbad Member in the hingeline area, but as the lower-energy mudstones also increase, secondary fracturing, rather than leached allochems, will become the critical factor controlling porosity.

Dolomite of lithofacies E represents the best potential reservoir rocks in the study area. Many of these rocks are stained almost black by petroleum residue and freely bled oil when placed on hot plates at 170° F. Intercrystalline and oomoldic or pelmoldic porosity (figs. 27, 30) are present in virtually every thin section, and porosity estimates run as high as 20 percent. Unfortunately, field data indicate lithofacies E becomes more important as the Sinbad thins to the southeast (fig. 3), away from potential subsurface production. Overall, however, the lithofacies maintains a thickness of from 6 to 6.5 m, and while it is likely this zone of dolomitization will persist along the regressive upper boundary of the Sinbad, it will probably not appreciably thicken.

As these porous dolomites pinch out basinward and are locally caught updip from oil migration, they create potential stratigraphic traps. Referring to his dolomitized calcarenite facies, which is roughly correlative with lithofacies E, Blakey (1977, p. 80) noted that the grainstone shoals are typically elongate and laterally bounded by muddier, poorly sorted sediments. Such a position also creates isolated stratigraphic traps on the depositional margins of the shoal.

Lithofacies F owes its presence to the relatively local effects of the Torrey delta sequence and probably does not extend any appreciable distance into the subsurface. This is unfortunate as the claystones of the lithofacies appear to have functioned as an effective local seal, against which hydrocarbons ponded in the upper units of the Sinbad.

In summary, this writer believes the Sinbad Limestone Member has considerable potential for oil and gas production, primarily in the hingeline area of central Utah, where it is faulted into the subsurface, overlain by an evaporite seal, and adjacent to probable source beds. The potential is increased by the probability of stratigraphic, as well as structural, traps. Porosity in the study area is all secondary, influenced mainly by dolomitization and selective leaching. Porosity encountered in hingeline, however, will probably be more dependent on fracturing.

APPENDIX

Section	*Name*	*Location*
1.	Grover	SW ¼, section 29, T. 29 S, R. 5 E
2.	Torrey	NE ¼, section 20, T. 29 S, R. 5 E
3.	Sulphur Creek	NW ¼, section 11, T. 29 S, R. 5 E
4.	Chimney Rock	SE ¼, section 7, T. 29 S, R. 6 E
5.	Monas Falls	Center, section 16, T. 29 S, R. 6 E
6.	Fremont River	NW ¼, section 22, T. 29 S, R. 6 E
7.	Cuts Canyon	NE ¼, section 27, T. 29 S, R. 6 E
8.	Grand Wash	SW ¼, section 35, T. 29 S, R. 6 E
9.	Miners Mountain	NW ¼, section 11, T. 30 S, R. 6 E
10.	Capitol Wash	SW ¼, section 13, T. 30 S, R. 6 E
11.	Pleasant Creek	SE ¼, section 30, T. 30 S, R. 6 E
12.	South Draw	NW ¼, section 6, T. 31 S, R. 7 E

REFERENCES CITED

Asquith, G. B., 1979, Subsurface carbonate models: a concise review: Petroleum Publishing, Tulsa, Oklahoma, 120p.

Bahr, C. W., 1963, Virgin Oil Field, Washington County, Utah: Intermountain Association of Petroleum Geologists, 12th Field Conference, p. 169–70.

Bathurst, R. G. C., 1975, Carbonate sediments and their diagenesis, Developments in Sedimentology 12: Elsevier, New York, 657p.

Belnap, D. W., 1971, Petrology and geochemistry of shoal water carbonates of the Virgin Limestone Member, Triassic Moenkopi Formation, Clark County, Nevada: Brigham Young University Geology Studies, v. 18, pt. 1, p. 147–84.

Bissell, H. J., 1970, Petrology and petrography of Lower Triassic marine carbonates of southern Nevada: E. J. Brill, Leiden, 24p.

Black, M., 1933, The algal sediments of Andros Island, Bahamas: Transactions of the Philosophical Society of London, series B., v. 222, p. 165–92.

Blakey, R. C., 1974, Stratigraphic and depositional analysis of the Moenkopi Formation, southeastern Utah: Utah Geological and Mineralogical Survey Bulletin 104, 81p.

———, 1977, Petroliferous lithosomes in the Moenkopi Formation, southern Utah: Utah Geology, v. 4, no. 2, p. 67–85.

Braun, M., and Friedman, G. M., 1969, Carbonate lithofacies and environments of the Tribe Hill Formation (Lower Ordovician) of the Mohawk Valley, New York: Journal of Sedimentary Petrology, v. 39, p. 113–35.

Chilingar, G. V., Zenger, D. H., Bissell, H. J., and Wolf, K. H., 1979, Dolomites and dolomitization: In Larden, G., and Chilingar, G. V. (eds.), Diagenesis in sediments and sedimentary rocks: Elsevier, New York, p. 423–536.

Deffeyes, K. S., Lucia, F. J., and Weyl, P. K., 1965, Dolomitization of Recent and Plio-Pleistocene sediments by marine evaporite waters on Bonaire, Netherlands, Antilles: In Pray, L. C., and Murray, R. C. (eds.), Dolomitization and limestone diagenesis, a symposium: Society of Economic Paleontologists and Mineralogists Special Publication 13, p. 71–88.

Dietz, R. S., and Holden, J. C., 1970, The breakup of Pangea: Scientific American, v. 223, no. 4, p. 30–41.

Dunham, R. J., 1962, Classification of carbonate rocks according to depositional texture: In Ham, W. E. (ed.), Classification of carbonate rocks: a symposium: American Association of Petroleum Geologists Memoirs 1, p. 108–21.

Evamy, B. D., 1973, The precipitation of aragonite and its alteration to calcite on the Trucial Coast of the Persian Gulf: In Purser, B. H. (ed.), The Persian Gulf, Holocene carbonate sedimentation and diagenesis in a shallow epicontinental sea: Springer-Verlag, New York, p. 329–41.

Evans, G., Murray, J. W., Biggs, N. E. J., Gate, R., and Bush, P. R., 1973, The oceanography, ecology, sedimentation, and geomorphology of parts of the Trucial Coast barrier island complex, Persian Gulf: In Purser, B. H. (ed.), The Persian Gulf, Holocene carbonate sedimentation and diagenesis in a shallow epicontinental sea: Springer-Verlag, New York, p. 233–77.

Folk, R. L., 1962, Spectral subdivision of limestone types: Ham, W. E. (ed.), Classification of carbonate rocks, a symposium: American Association of Petroleum Geologists Memoir 1, p. 62–84.

———, 1965, Some aspects of recrystallization in ancient limestones: In Pray, L. C., and Murray, R. C. (eds.), Dolomitization and limestone diagenesis, a symposium: Society of Economic Paleontologists and Mineralogists Special Publication 13, p. 14–48.

———, 1974, The natural history of crystalline calcium carbonate; effect of magnesium content and salinity: Journal of Sedimentary Petrology, v. 44, p. 40–53.

Friedman, G. M., 1959, Identification of carbonate minerals by staining methods: Journal of Sedimentary Petrology, v. 29, p. 87–97.

Gilluly, J., and Reeside, J. B., 1928, Sedimentary rocks of the San Rafael Swell and some adjacent areas in eastern Utah: U.S. Geological Survey Professional Paper 150-D, p. 61–110.

Ginsburg, R. N., Rezak, R., and Wray, J. L., 1972, Geology of calcareous algae: Sedimenta 1, University of Miami, Miami, Florida, 66p.

Hanshaw, B. B., Back, W., and Deike, R. G., 1971, A geochemical hypothesis for dolomitization by ground water: Economic Geology, v. 66, p. 710–24.

Hawley, C. C., Robeck, R. C., and Dyer, H. B., 1968, Geology, altered rocks and ore deposits of the San Rafael Swell, Emery County, Utah: U.S. Geological Survey Bulletin 1239, 115p.

Heckel, P. H., 1972, Recognition of ancient shallow marine environments: In Rigby, J. K., and Hamblin, W. K. (eds.), Recognition of ancient sedimentary environments: Society of Economic Paleontologists and Mineralogists Special Publication 16, p. 226–86.

Hintze, L. F., 1973, Geologic history of Utah: Brigham Young University Geology Studies, v. 20, pt. 3, 181p.

Hsü, K. J., and Schneider, J., 1973, Progress report on dolomitization-hydrology of Abu Dhabi sabkhas, Arabian Gulf: In Purser, B. H. (ed.), The Persian Gulf, Holocene carbonate sedimentation and diagenesis in a shallow epicontinental sea: Springer-Verlag, New York, p. 409–22.

Hunt, C. B. (assisted by P. Averitt and R. L. Miller), 1953, Geology and geography of the Henry Mountains region, Utah: U.S. Geological Survey Professional Paper 228, 234p.

Illing, L. V., Wells, A. J., and Taylor, J. C. M., 1965, Penecontemporary dolomite in the Persian Gulf: In Pray, L. C., and Murray, R. C. (eds.), Dolomitization and limestone diagenesis: a symposium: Society of Economic Paleontologists and Mineralogists Special Publication 13, p. 89–111.

Jacka, A. D., and Franco, L. A., 1975, Deposition and diagenesis of Permian evaporites and associated carbonates and clastics on shelf areas of the Permian Basin: In 4th Symposium on Salt, Northern Ohio Geological Society, Cleveland, Ohio, p. 67–89.

James, N. P., 1979, Shallowing upward sequences in carbonates: In Walker, R. G. (ed.), Facies models: Geoscience Canada, Reprint Series 1, p. 109–19.

Kendall, A. C., 1979, Continental and supratidal (sabkha) evaporites: In Walker, R. G. (ed.), Facies models: Geoscience Canada, Reprint Series 1, p. 145–57.

Kennedy, W. J., 1975, Trace fossils in carbonate rocks: In Frey, R. W. (ed.), The study of trace fossils: Springer-Verlag, New York, p. 377–98.

Kinsman, D. J., 1969, Modes of formation, sedimentary associations, and diagnostic features of shallow-water and supratidal evaporites: American Association of Petroleum Geologists Bulletin, v. 53, p. 830–40.

Koch, W. J., 1976, Lower Triassic facies in the vicinity of the Cordilleran hingeline: western Wyoming, southeastern Idaho, and Utah: Rocky Mountain Association of Geologists 1976 Symposium, p. 203–17.

Kummel, B., 1954, Triassic stratigraphy of southeastern Idaho and adjacent areas: U.S. Geological Survey Professional Paper 254-H, p. 165–94.

Land, L. S., 1973, Holocene meteoric dolomitization of Pleistocene limestones, North Jamaica: Sedimentology, v. 20, p. 411–24.

Logan, B. W., Rezak, R., and Ginsburg, R. N., 1964, Classification and environmental significance of algal stromatolites: Journal of Geology, v. 12, p. 68–83.

Loreau, J. P., and Purser, B. H., 1973, Distribution and ultrastructure of Holocene ooids in the Persian Gulf: In Purser, B. H. (ed.), The Persian Gulf, Holocene carbonate sedimentation and diagenesis in a shallow epicontinental sea: Springer-Verlag, New York, p. 279–328.

Lucia, F. J., 1972, Recognition of evaporite-carbonate shoreline sedimentation: In Rigby, J. K., and Hamblin, W. K. (eds.), Recognition of ancient sedimentary environments: Society of Economic Paleontologists and Mineralogists Special Publication 16, p. 160–91.

McKee, E. D., 1954, Stratigraphy and history of the Moenkopi Formation: Geological Society of America Memoir 61, 133p.

Moulton, F. C., 1976, Lower Mesozoic and upper Paleozoic petroleum potential of the hingeline area, central Utah: Rocky Mountain Association of Geologists 1976 Symposium, p. 219–29.

Murray, R. C., 1960, Origin of porosity in carbonate rocks: Journal of Sedimentary Petrology, v. 31, p. 59–84.

Newell, N. D., Imbrie, J., Purdy, E. G., and Thurber, D. L., 1959, Organism communities and bottom facies, Great Bahama Bank: Bulletin American Museum of Natural History, v. 117, p. 117–228.

Newell, N. D., Rigby, J. K., Fischer, A. B., Whiteman, A. J., Hickox, J. E., and Bradley, J. S., 1953, The Permian reef complex of the Guadalupe Mountains region, Texas and New Mexico: W. H. Freeman, San Francisco, 236p.

Newman, D. H., 1974, Paleoenvironment of the Lower Triassic Thaynes Formation near Cascade Springs, Wasatch County, Utah: Brigham Young University Geology Studies, v. 21, pt. 3, p. 63–96.

Playford, P. E., and Cockbain, A. E., 1969, Algal stromatolites–deep-water forms in the Devonian of Western Australia: Science, v. 165, p. 1008–10.

Purdy, E. G., 1961, Bahamian oolite shoals, In Peterson, J. A., and Osmond, J. C. (eds.), Geometry of sandstone bodies: American Association of Petroleum Geologists, p. 53–62.

———, 1963, Recent calcium carbonate facies of the Great Bahama Bank: Journal of Geology, v. 71, p. 334–35, 472–97.

Purser, B. H., and Evans, G., 1973, Regional sedimentation along the Trucial Coast, SE Persian Gulf, In Purser, B. H. (ed.), The Persian Gulf, Holocene carbonate sedimentation in a shallow epicontinental sea: Springer-Verlag, New York, p. 211–32.

Reineck, H. E., and Singh, I. B., 1975, Tidal flats: In Depositional sedimentary environments: Springer-Verlag, New York, p. 355–72.

Rigby, J. K., 1967, Triassic lyssakid sponges from Utah: Geological Society of America Abstracts, no. 101, p. 178.

Sabins, F. F., Jr., 1962, Grains of detrital, secondary, and primary dolomite from Cretaceous strata of the western interior: Geological Society of America Bulletin, v. 73, p. 1183–96.

Sarjeant, W. A., 1975, Plant trace fossils: In Frey, R. W. (ed.), The study of trace fossils: Springer-Verlag, New York, 562p.

Schmalz, R. F., 1969, Deep-water evaporite deposition: a genetic model: American Association of Petroleum Geologists Bulletin, v. 53, p. 798–823.

Schneider, J. F., 1975, Recent tidal deposits, Abu Dhabi, UAE, Arabian Gulf: In Ginsburg, R. N. (ed.), Tidal deposits: A casebook of recent examples and ancient counterparts: Springer-Verlag, New York, p. 209–14.

Scholle, P. A., 1978, Carbonate rock constituents, textures, cements, and porosities: American Association of Petroleum Geologists Memoir 27, 241p.

Seilacher, A., 1967, Bathymetry of trace fossils: Marine Geology, v. 5, p. 413–28.

Sellwood, B. W., 1978, Shallow-water carbonate environment: In Reading, H. G. (ed.), Sedimentary environments and facies: Elsevier, New York, p. 259–313.

———, 1973, Carbonate coastal accretion in an area of longshore transport, NE Qatar, Persian Gulf: In Purser, B. H. (ed.), The Persian Gulf,

Holocene carbonate sedimentation and diagenesis in a shallow epicontinental sea: Springer-Verlag, New York, p. 179–92.

Shinn, E. A., Ginsburg, R. N., and Lloyd, R. M., 1965, Recent supratidal dolomite from Andros Island, Bahamas: In Pray, L. C., and Murray, R. C. (eds.), Dolomitization and limestone diagenesis: a symposium: Society of Economic Paleontologists and Mineralogists Special Publication 13, p. 112–23.

Shinn, E. A., Lloyd, R. M., and Ginsburg, R. N., 1969, Anatomy of a modern carbonate tidal flat: Journal of Sedimentary Petrology, v. 39, no. 3, p. 1202–1228.

Smith, D. B., 1974, Origin of tepees in Upper Permian shelf carbonate rocks of Guadalupe Mountains, New Mexico: American Association of Petroleum Geologists Bulletin, v. 58, p. 63–70.

Smith, J. F., Huiff, L. C., Hinrichs, E. N., and Leudke, R. B., 1963, Geology of the Capitol Reef area, Wayne and Garfield Counties, Utah: U.S. Geological Survey Professional Paper 363, 102p.

Spencer, C. W., 1975, Petroleum geology of east-central Utah and suggested approaches to exploration: Four Corners Geological Society Guidebook, 8th Field Conference, Canyonlands, p. 263–75.

Stewart, J. H., Poole, F. B., and Wilson, R. F., 1972, Stratigraphy and origin of the Triassic Monkeopi Formation and related strata in the Colorado Plateau region: U.S. Geological Survey Professional Paper 691, 195p.

Tasch, P., 1973, Paleobiology of the invertebrates: data retrieval from the fossil record: John Wiley and Sons, New York, 946p.

Wagner, C. W., and Van Der Togt, C., 1973, Holocene sediment types and their distribution in the southern Persian Gulf: In Purser, B. H. (ed.), The Persian Gulf, Holocene carbonate sedimentation and diagenesis in a shallow epicontinental sea: Springer-Verlag, New York, p. 123–56.

Wilson, J. L., 1975, Carbonate facies in geologic history: Springer-Verlag, New York, 471p.

EXPLANATION OF PLATE 1

FIGURES 1–5.–Ammonoids from lithofacies D of the Sinbad Limestone Member: 1.–*Wyomingitis* sp., 2–4.–*Meekoceras* sp., 5.–Slab with ammonoid coquina of mainly *Meekoceras* sp. All ammonoids showing X1. FIGURES 6–7.–Representative gastropods from the Sinbad member. X1. FIGURE 8.–Slab of bivalves from unit 42, Torrey section, showing typical *Myalina-Pleuromya* suite. FIGURE 9.–Slab of bivalves from unit 41, Chimney Rock section showing typical *Aviculopectin* suite.


1


2


3

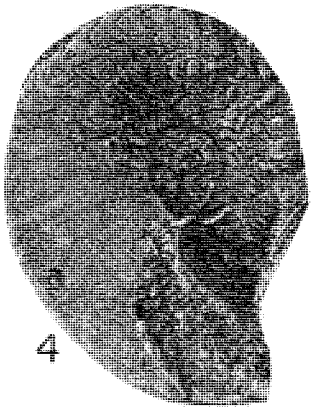
4

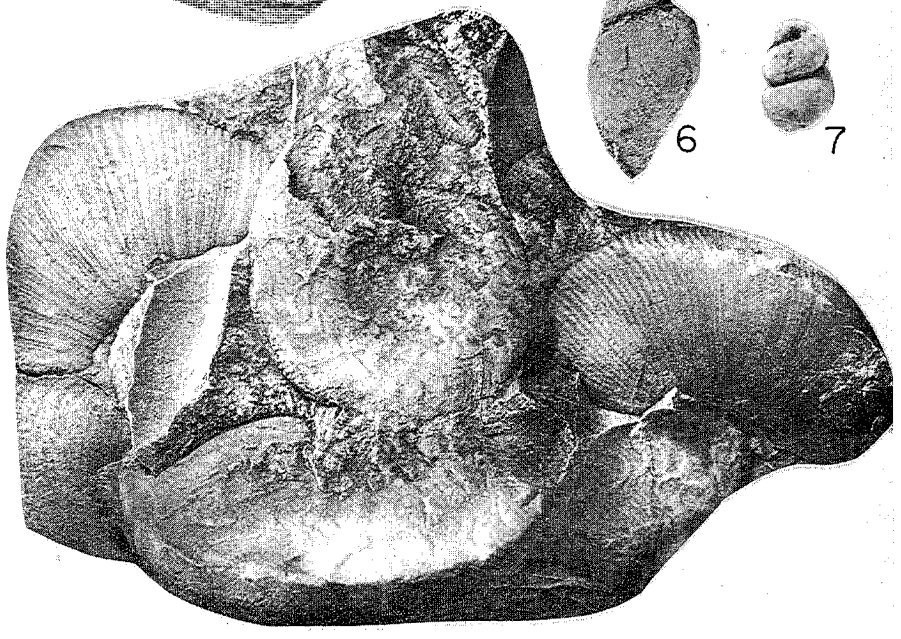
5


6

7

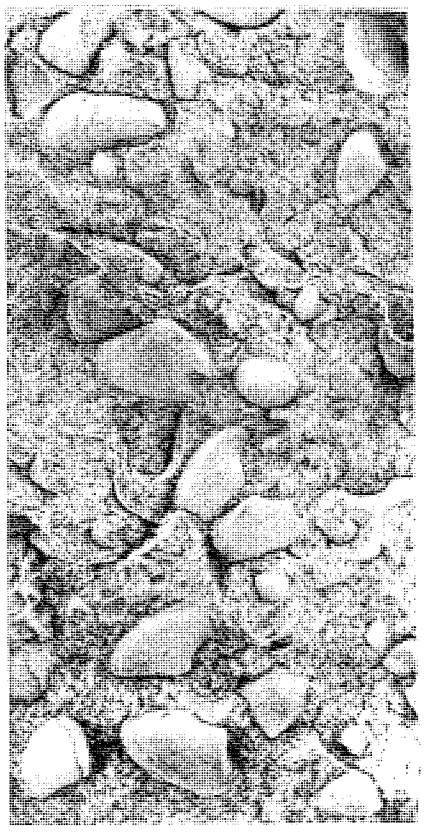
8

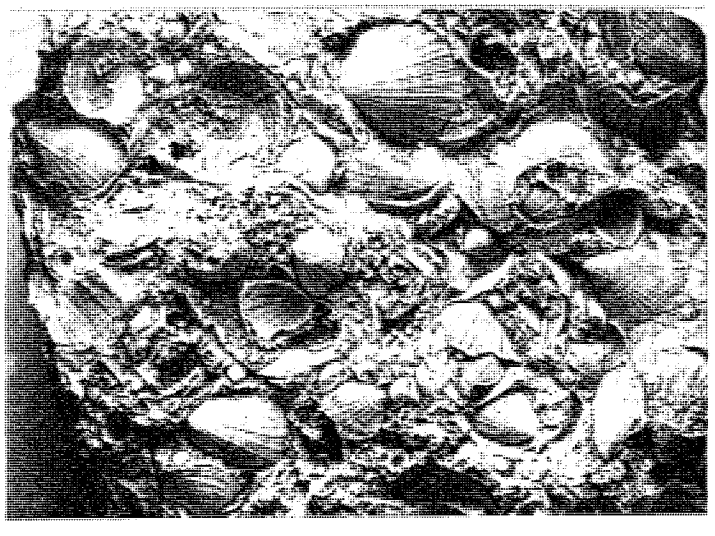
9

EXPLANATION OF PLATE 2

FIGURES 1, 3, and 4.–Typical bioturbation found in the Sinbad Limestone Member: 1,3.–*Planolites, Skolithos,* and assorted feeding traces from channel bottoms of lithofacies C, unit 35, Torrey section. 4.–Casts of burrowing bivalves from unit 44, Monas Falls section, figures 1, 3 X2; figure 4 X1. FIGURE 2.–Lyssakid sponge preserved as limonite stain from unit 39, Torrey section. Note tubular shape and frilled outline. X1.5. FIGURE 5.–Close-up view of spicule net from figure 2, showing diagonal overlapping of poorly preserved skeletal elements, X5.

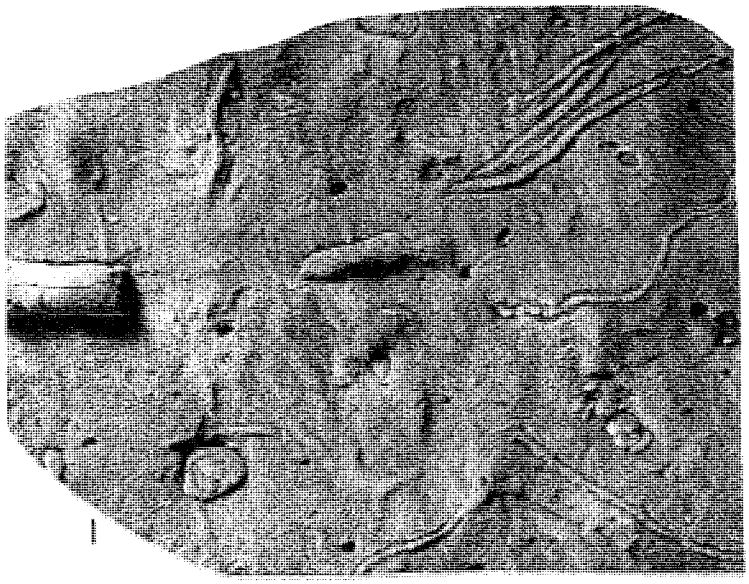

1

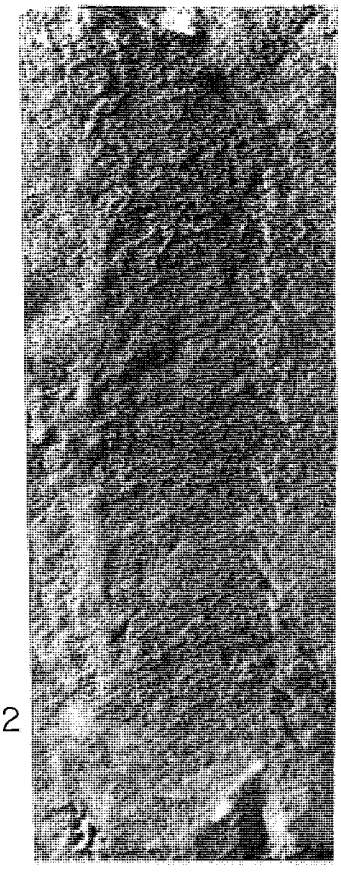

2

3

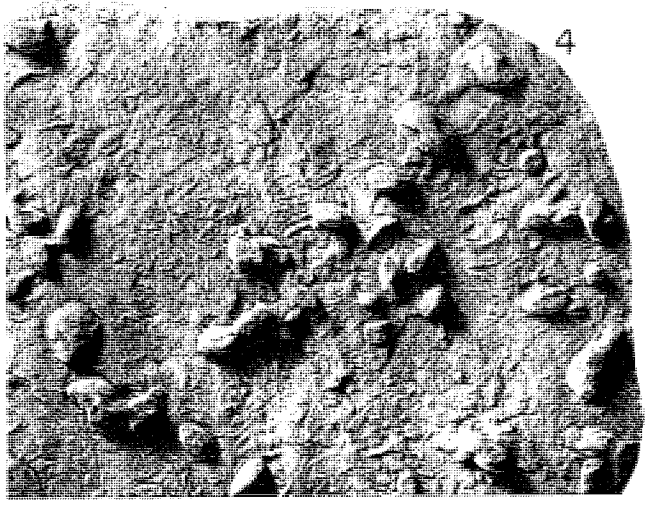

4

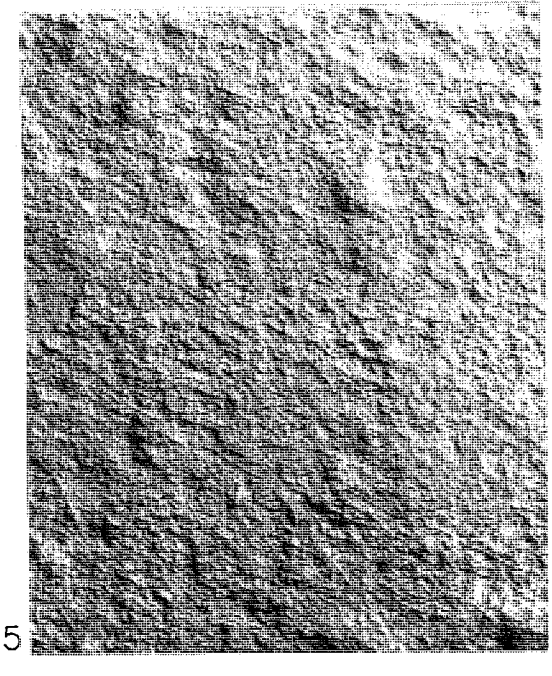

5